POLYMER NANOPARTICLES AS A DEGRADABLE, MUCOADHESIVE DRUG DELIVERY SYSTEM

POLYMER NANOPARTICLES AS A DEGRADABLE, MUCOADHESIVE DRUG DELIVERY SYSTEM

By

NICOLE MANGIACOTTE, B.ENG.BIOSCIENCES.

A Thesis

Submitted to the School of Graduate Studies

In the Partial Fulfillment of the Requirements

For the Degree

Master of Applied Science

McMaster University

MASTER OF APPLIED SCIENCE (2016) McMaster University

(Chemical Engineering) Hamilton, Ontario

TITLE: Polymer Nanoparticles as a Degradable, Mucoadhesive Drug Delivery System

AUTHOR: Nicole Mangiacotte, B. Eng. & Biosci. (McMaster University)

SUPERVISOR: Professor Heather Sheardown

NUMBER OF PAGES: xi, 56

ABSTRACT

One of the most common methods of drug delivery to the anterior segment of the eye is topical application of an ophthalmic solution or suspension. The ophthalmic solution may contain various particle based materials, such as nanoparticles, to control the rate at which the drug is delivered to the eye. The issue with this delivery method is that there are several barriers at the front of the eye. These barriers, which include a high tear film turnover rate and induced lacrimation, reduce the residence time of the drug at the site of administration and result in 95% of the administered drug being removed systemically or via nasolacrimal drainage. Additionally, once the material has left the target location it should degrade in a controlled manner so that it can be safely removed from the body.

The current work focuses on the development of polymeric nanoparticles that can serve as a delivery system for ophthalmic drugs. The material proposed for the nanoparticle synthesis is poly(2-hydroxyethyl methacrylate (HEMA)), a polymer with a long history of ophthalmic compatibility. The original nanoparticle formulation was modified to allow for degradation and mucoadhesion. To facilitate degradation, a crosslinker which degrades under ocular conditions was incorporated. A mucoadhesive polymer was incorporated into the particles to enhance the residence time of the particles at the front of the eye.

Size and morphology analysis of the final polymer products showed that nano-sized, spherical particles were produced. FTIR spectra demonstrated that the nanoparticles were comprised of poly(HEMA) and that 3-(acrylamido)phenylboronic acid

(3AAPBA) was successfully incorporated. Degradation of nanoparticles containing N,N'-bis(acryloyl)cystamine (BAC) after incubation with DL-dithiothreitol (DTT) was confirmed by a decrease in turbidity, measured by absorbance, and through transmission electron microscopy (TEM). Based on zeta potential results, poly(HEMA, BAC, 3AAPBA) samples C3 to C6 were found to be mucoadhesive. Dexamethasone release from poly(HEMA) nanoparticles and poly(HEMA, BAC, 3AAPBA) nanoparticles, loaded with efficiencies of 15.0% ±1.4% and 5.3% ±0.4%, resulted in rate constants of 0.001 and 0.002, and release exponents of 0.607 and 0.586, respectively. The toxicity of the nanoparticles was tested by incubation in the presence of human corneal epithelial cells (HCEC). In the presence of the poly(HEMA), poly(HEMA, BAC), and poly(HEMA, BAC, 3AAPBA) samples the HCEC viability was found to be 123.6% to 182.5%, 88.5% to 111%, and 69.8% to 85.1%, respectively. The viability of HCEC after incubation with poly(HEMA) was significantly higher compared to poly(HEMA, BAC) samples with a dilution factor of 0 and 2. Additionally, the HCEC viability in the presence of poly(HEMA, BAC, 3AAPBA) sample C6 was found to be significantly lower compared to samples C2 and C3 from Table 3. The previously summarized results suggest that the poly(HEMA) based nanoparticles produced in this work have the potential for drug delivery to the front of the eye.

ACKNOWLEDGEMENTS

First of all I would like to thank my supervisor Dr. Heather Sheardown for taking a chance on me when I was only one of many second year students in her class. Thank you for your all of the encouragement and advice that you gave me. It helped me to keep motivated and moving forward with my research. Your support gave me the confidence I needed to pursue my Master's degree.

Next I would like to thank my parents and my sister for supplying me with a constant stream of encouragement and for never letting me give up on myself. You were all there to listen to me when I needed you, which was more often than I'd like to admit. You earned this degree as much as I did.

To my engineering family, especially Helen and Robin, thank you for being wonderful human beings and for making Hamilton feel like my home away from home. You truly are a special group of people and I am lucky to call you my friends.

Finally, I would like to extend a big thank you to everyone in the Sheardown lab group for your valuable input and support. Special thanks to Lina for helping me start my project, Graeme and Marion for all the experiments you helped me run and for offering suggestions every time I hit a wall, Megan for all of your help with cell work, and Cheryl for your TEM expertise.

TABLE OF CONTENTS

LIST OF FIGURES

LIST OF TABLES

LIST OF ABBREVIATIONS

HEMA	2-hydroxyethyl methacrylate
EGDMA	Ethylene glycol dimethacrylate
MAA	Methacrylic acid
SDS	Sodium dodecyl sulfate
BPO	Benzoyl peroxide
BAC	N,N'-Bis(acryloyl)cystamine
3AAPBA	3-(acrylamido)phenylboronic acid
MWCO	Molecular weight cut off
DLS	Dynamic light scattering
TEM	Transmission electron microscopy
DTT	DL-Dithiothreitol
KCl	Potassium chloride
FTIR	Fourier transform infrared spectroscopy
ATR-FTIR	Attenuated total reflectance fourier transform infrared spectroscopy
KBr	Potassium bromide
HCEC	Human corneal epithelial cells
KSFM	Keratinocyte serum free medium
DMSO	Dimethyl sulfoxide
PBS	Phosphate buffered saline

1. INTRODUCTION

1.1. Nanoparticles as Ocular Drug Delivery Systems

The main issue with ocular drug delivery through topically applied solutions is that there are several barriers at the front of the eye that trap and rapidly remove foreign substances (Gaudana, Ananthula, et al. 2010). These include pre-corneal barriers, such as mucin in the tear film and induced lacrimation, and the corneal epithelium, which serves as a mechanical barrier (Garhart and Lakshminaravanan 2012; Gaudana, Ananthula, et al. 2010; Ghate and Edelhauser 2006; Urtti 2006). Due to the presence of these barriers, 95% of drugs that are administered topically are removed systemically or via nasolacrimal drainage (Gaudana, Ananthula, et al. 2010; Urtti 2006).

Particle delivery systems within the size range of 10 nm to 1000 nm are commonly referred to as nanoparticles (Bucolo, Drago, et al. 2012). Nanoparticles have the potential to improve the delivery of hydrophobic drugs, target specific cells or tissues for drug delivery, and transport drugs across tight epithelial and endothelial barriers (Farokhzad and Langer 2009). Other reasons why nanoparticles are attractive for use as drug delivery systems are that they assist in the stabilization of drugs for release and can control the rate of drug release (Soppimath, Aminabhavi, et al. 2001).

Topical administration of nanoparticles may result in sustained drug release and therapeutic effect if the nanoparticles are retained in the eye (Bucolo, Drago, et al. 2012). If the formulation is not retained in the eye for a sufficient period of time, more frequent pulse type dosing at a high concentration is required, which may result in detrimental side effects (Kaur, Garg, et al. 2004). Therefore, the frequency of dosing can be reduced by

increasing the residence time of the nanoparticles in the eye. Less frequent dosing is associated with a reduction in toxicity and maintenance of therapeutic effect (De Jong and Borm 2008). Additionally, patient compliance is higher when the dosage frequency is decreased (Ghate and Edelhauser 2006). The residence time may be increased by creating interactions with the ocular mucosa through the incorporation of mucoadhesive materials into the nanoparticles. Mucoadhesive materials are able to form non-covalent bonds with the mucin coat over the corneal surface, resulting in intimate contact between the surface of the eye and the drug loaded nanoparticles (Kaur, Garg, et al. 2004).

Polymer based nanoparticles should biodegrade over time in the body so that there is minimal to no long term impact due to the presence of a foreign material. Degradation of the particles may take place after the nanoparticles have released drug at the front of the eye and been removed systemically. Once the nanoparticles are removed from the eye they are no longer therapeutically useful (Deshayes and Kaska 2013). The degradation products should then be easily eliminated from the body (Azevedo and Reis 2005).

1.2. Overall Objectives

The overall objectives of the research summarized in this thesis revolve around the creation of novel nano-sized polymer particles. The polymer selected for nanoparticle synthesis should be ophthalmically compatible. It is preferred that the nanoparticles have a maximum diameter of 200 nm. Additional requirements for the nanoparticles include the ability to load and release an ophthalmic drug and to degrade under reducing conditions. The nanoparticles should have a mucoadhesive component to increase the

residence time of the drug delivery system at the front of the eye. This will allow an increased amount of drug to be released in the desired location.

1.3. Thesis Outline

The work in this thesis was organized into five chapters. Chapter 1 introduces the topic of the thesis and the objectives of the research, along with this outline. The literature review is included in Chapter 2 and focuses on various aspects of drug delivery systems, the preparation and application of poly(2-hydroxyethyl methacrylate) nanoparticles, and the overview, application, and incorporation of mucoadhesive components. The materials and methods used during the research work are discussed in Chapter 3. The results and discussion, more specifically the size, composition, and morphology of the nanoparticles and their degradation and mucoadhesive characteristics, are summarized in Chapter 4. Finally, Chapter 5 contains concluding statements and recommendations for future experimentation.

2. LITERATURE REVIEW

2.1. Anatomy of the Anterior Eye

The components of the eye can be separated into two sections, the interior and exterior eye. The exterior eye is comprised of the cornea, sclera, and limbus. The cornea is transparent, avascular, and refracts light entering the eye, whereas the sclera is fibrous tissue that is opaque and white. The limbus is the border of the two previously mentioned tissues (Atchison 2000; Kiel 2010). The interior eye is further separated into two sections, the anterior and posterior segments. The cornea, iris, ciliary body, lens, and anterior chamber are all part of the anterior segment (Kiel 2010). The iris consists of two muscles that change the size of its aperture through opposing actions (Purves, Augustine, et al. 2001). The ciliary body is a circular tissues connected to the lens by suspensory ligmanents, called zonules, that assists with changing the focus of the image captured by the eye (Atchison 2000). The lens is a transparent biconcave disc surrounded by an elastic capsular bag (Smerdon 2000). It is also able to refract light but with a lower power relative the cornea. The power of refraction is modified by the lens in order to change the focus to view objects at different distances (Atchison 2000). Aqueous humor, which fills the anterior chamber, is a transparent liquid that supplies nutrients to the surrounding structures and maintains the intraocular pressure in the eye. Uptake of this liquid occurs at the junction between the iris and the cornea (Garhart and Lakshminaravanan 2012; Purves, Augustine, et al. 2001).

The arterial supply to the eye comes from a branch of the internal carotid artery called the ophthalmic artery. The ophthalmic artery enters with the optic nerve into the

orbit and branches off into several different arteries that supply the eye. These arteries include the lacrimal artery, anterior and posterior ethmoidal branches, and the dorsalis nasal artery. The lacrimal glands in the eyelids, sinuses and nasal cavity, and lacrimal sac and root of the nose are supplied by the lacrimal artery, anterior and posterior ethmoidal branches, and dorsalis nasal artery, respectively. The venous system starts with the superior ophthalmic vein that originates at the root of the nose and follows the path of the ophthalmic artery. Two main segments are the inferior ophthalmic vein and the angular vein, the latter of which travels down the side of the nasal bridge (Smerdon 2000).

2.2. Anterior Eye Diseases

Conjunctivitis, dry eye, glaucoma, and anterior uveitis are all examples of diseases that affect the front of the eye (Alvarez-Lorenzo, Yanez, et al. 2006; Lee, Hughes, et al. 2010). Conjunctivitis can be categorized into non-infectious causes, such as allergic reaction, or infectious causes, such as bacteria or viruses. It is one of many diseases that cause redness in the eye (Azari and Barney 2013). General features of conjunctivitis include dilated conjunctival vessels, a milky appearance of the conjunctiva, and discharge from the eye (Azari and Barney 2013; Friedlaender 1993). The type of discharge and certain symptoms vary based on the cause of conjunctivitis (Azari and Barney 2013).

The two main classes of dry eye are aqueous tear-deficient dry eye and evaporative dry eye. The primary cause of aqueous tear-deficient dry eye is lack of lacrimal tear secretion by itself or in combination with lack of water secretion by the conjunctiva. In contrast, evaporative dry eye is not associated with any issues in secretion but rather increased water loss from the ocular surface (Lemp and Foulks 2007).

Symptoms of dry eye include discomfort, burning, foreign-body sensation, visual disturbance, and tear film instability. These symptoms become worse in dry, cold, or windy environments, as well as during periods of decreased blinking, due to increased evaporation from the ocular surface (Azari and Barney 2013; Lemp and Foulks 2007).

Glaucoma is a disease characterized by an optic nerve with structural damage and related visual dysfunction. The characteristic defects to the visual field associated with early to moderate cases of glaucoma include assymetrical defects across the horizontal midline and defects in the mid-periphery (Foster, Buhrmann, et al. 2002). The two types of primary glaucoma, meaning it was not caused by another condition, are open and closed angle. These names refer to the configuration of the irido-corneal angle in the affected eye. Aside from cases with narrow angles that may experience some pain, the only symptom is visual loss (Leske 1983).

Uveitis is a general term rather than a reference to a specific disease, for the inflammation of the choroid, iris, and ciliary body. Anterior uveitis means that the inflammation is in the anterior segment of the eye (McCannel, Holland, et al. 1996). The inflammation of these structures can result in pain and blurred vision in the affected eye (Azari and Barney 2013). Anterior eye drug delivery is an important part of treatment for the previously mentioned anterior eye diseases, as well as many others.

2.3. Anterior Eye Drug Delivery Systems

2.3.1. Routes of Administration

The major routes of drug delivery to the anterior eye are topical and subconjunctival (Gaudana, Ananthula, et al. 2010; Ghate and Edelhauser 2006). For

topical delivery, eye drops are the most commonly used form (Gaudana, Ananthula, et al. 2010; Urtti 2006). Eye drops are an attractive method of drug delivery because they are self-administrable and non-invasive (Gaudana, Ananthula, et al. 2010). The eye drop solutions may be made up of a variety of particle based materials, such as liposomes, microemulsions, nanoparticles, and nanoemulsions, which contain an ocular drug that is dissolved, entrapped, encapsulated, adsorbed or attached (Gaudana, Ananthula, et al. 2010; Ghate and Edelhauser 2006). The reason for incorporating particles in topical drug delivery systems is that they provide continuous controlled drug release, which results in less frequent administration, and the ability to pass through blood-ocular barriers (Gaudana, Ananthula, et al. 2010). Subconjunctival delivery tries to extend the time in between dosages and provide sustained drug levels. Another benefit is that the drug does not have to pass through the conjunctival epithelium, which is difficult for hydrophilic drugs. However, the main issue with this method is that repeat injections are associated with ocular morbidity, especially for inflamed eyes (Ghate and Edelhauser 2006). The delivery method selected for this project was a topical eye drop solution containing nanoparticles because of the benefits in terms of ease of use and controlled release.

2.3.2. Biological Barriers in the Eye

There are several barriers that they body has in place to protect foreign substances from entering the eye. The first set of barriers, present anterior to the cornea, consist of blinking, the tear film and its turnover rate, drainage, and induced lacrimation. Turnover of the tear film, produced from lacrimal glands in the eyelids, occurs every 2 to 3 minutes resulting in the topical solution being washed away. Additionally, the tear film contains

mucin that forms a hydrophilic layer, which traps debris and pathogens (Garhart and Lakshminaravanan 2012; Gaudana, Ananthula, et al. 2010). An increase in tear volume, due to the presence of an irritant or the application of eye drops, results in rapid reflex blinking and the subsequent movement of the drug into the drainage system or out of the eye and onto the face (Ghate and Edelhauser 2006). Due to the flow in the eye being directed to the nasal cavity and capillaries local to the conjunctival sac 95% of drug administered is removed systemically and only 5% or less is able to reach intraocular tissues (Gaudana, Ananthula, et al. 2010; Urtti 2006).

Next in line is the cornea, which has an outer layer of epithelium that acts as a mechanical barrier (Gaudana, Ananthula, et al. 2010; Ghate and Edelhauser 2006; Urtti 2006). The corneal epithelium is lipophilic and is responsible for 90% and 10% of the barrier to hydrophilic or lipophilic drugs, respectively. Hydrophilic drugs generally pass between the cells of the epithelium and lipophilic drugs generally pass through the cells of the epithelium. However, this barrier is weakened when the cornea is diseased (Ghate and Edelhauser 2006).

2.3.3. Methods for Improved Delivery

There are a few different approaches that have been considered for improve drug delivery to the anterior segment of the eye. The two general categories for improvement methods are modification of the drug and the delivery system. Modifications of the drug include altering the solubility and lipophilicity, as well as corneal epithelium transporter targeting materials (Gaudana, Ananthula, et al. 2010). In terms of modifying the delivery system there are a few different approaches that can be taken. The type of formulation can

be changed from an eye drop to a gel, ointment, or an insert (Urtti 2006). Another approach is to modify the existing eye drop formulation by reducing the volume per dosage. Reducing the drop volume from 35 – 56 µl to 5 – 15 µl has the potential to increase the local/systemic drug ratio (Ghate and Edelhauser 2006). Finally, addition of mucoadhesive materials to the nanoparticles in the drops would help to extend the residence time of the drug delivery system in the eye (Kaur, Garg, et al. 2004). Due to the fact that nanoparticle design is the focus of this work, rather than the final administrable formulation, the addition of a mucoadhesive material was selected as the method for improving drug delivery to the front of the eye.

2.4. Poly(2-hydroxyethyl methacrylate (HEMA))

2.4.1. Properties of Poly(HEMA)

HEMA is a water-soluble monomer that contains a hydrophilic hydroxyl side group and is associated with low toxicity at low concentrations (1%). It can be easily polymerized and used to form a hydrogel (Montheard, Chatzopoulos, et al. 1992). The polymerized form, poly(HEMA), differs from the monomer because it is not water soluble regardless of crosslinking (Chirila, Constable, et al. 1993). The structure of the polymer can be found in Figure 1. Typically poly(HEMA) hydrogels have an approximate equilibrium hydration of 40% water content, which can be varied by changing the crosslinking density (Holly and Refojo 1975). Although these hydrogels are generally specified as porous materials, the porosity and associated properties are dependent on the polymerization technique. Bulk polymerization leads to a hard, glassy, transparent, relatively non-porous material that becomes soft and flexible in the presence

of water. Microporous and macroporous poly(HEMA), formed by polymerization in solution, is still transparent and water-swellable but with a reduced hardness relative to the non-porous material (Chirila, Constable, et al. 1993).

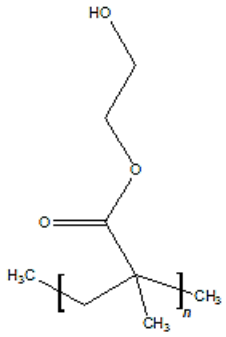

Figure 1. Chemical structure of poly(HEMA).

Poly(HEMA) is biologically inert, resistant to degradation, and is not damaged by the high heat and pressure from autoclave sterilization (Cadotte and DeMarse 2005). Studies have shown that poly(HEMA) is resistant to reactions involving amines and acid hydrolysis due to its high chemical stability (Peppas, Moyniham, et al. 1985). Additionally, poly(HEMA) is non-ionic resulting in high hemocompability (Cadotte and DeMarse 2005; Montheard, Chatzopoulos, et al. 1992). Therefore, there is delayed thrombus formation when poly(HEMA) is in the presence of blood (Montheard, Chatzopoulos, et al. 1992). Mammalian cells are unable to attach and grow on poly(HEMA) that has not been modified (Montheard, Chatzopoulos, et al. 1992).

2.4.2. Applications of Poly(HEMA)

There are many potential applications for poly(HEMA) because it has a similar density and water content compared to living tissue (Cadotte and DeMarse 2005). Poly(HEMA) was originally designed as an ophthalmic material and it remains a

significant part of the ophthalmology (Zaikov and Horák 2007). HEMA was one of the first hydrophilic monomers used for the synthesis of contact lenses. In terms of soft contact lenses, HEMA continues to be the most frequently used hydrophilic monomer (Nicolson and Vogt 2001). Soft contact lenses were originally designed to fix refractive errors. However, research has been conducted to expand their function to include drug delivery (Alvarez-Lorenzo, Yanez, et al. 2006). Poly(HEMA) based contact lenses can be made into drug delivery systems through the formation of reversible covalent bonds between the drug and the lens, integration of colloidal structures loaded with drug, or by direct interactions with the drug through the incorporation of a copolymer with specific functional groups (Alvarez-Lorenzo, Yanez, et al. 2006). In fact, there have been several studies conducted involving the incorporation of drug loaded nanoparticles into poly(HEMA) contact lenses (Gulsen and Chauhan 2004; Garhwal, Shady et al. 2012; Jung and Chauhan 2012; Phan, Subbaraman et al. 2014). Additionally, cyclodextrins have been incorporated in poly(HEMA) lenses for the release of poorly water soluble drugs. Cyclodextrins are useful because they can increase the stability of these drugs in aqueous solutions through the formation of inclusion complexes. The inclusion complexes are created by reversible non-covalent interactions between the cyclodextrins and the drug molecules (dos Santos, Alvarez-Lorenzo, et al. 2009; Xu, Li, et al. 2010).

Poly(HEMA) can also be used for ophthalmic applications when it is formed into a sponge. Proposed uses of these hydrogel sponges include drug delivery and artificial corneas. The pore flow and free volume diffusion of the sponge can be optimised to achieve a desirable drug uptake and release. For artificial corneas, poly(HEMA) sponges

are attractive because they can surround the central material and act as an anchor through ingrowth of specific cells (Chirila, Constable, et al. 1993; Lou, Munro, et al. 2004).

Other applications include wound dressing, breast implants, and soft tissue replacement (Dalton and Shoichet 2001; Vacanti 2004; Young, Wu, et al. 1998). For the purpose of advanced wound replacement, artificial skin was prepared from poly(HEMA) hydrogels reinforced by various fibers and fabrics (Young, Wu, et al. 1998). Poly(HEMA) can also be useful as a protective layer covering breast implants due to the fact it does not promote the formation of a fibrous capsule (Vacanti 2004). For soft tissue applications, poly(HEMA) can be formed into tubes which could be used to replace natural structures such as nerve guidance channels (Dalton and Shoichet 2001).

Poly(HEMA) has also been used to prepare nanoparticles. The applications of poly(HEMA) nanoparticles can be divided into two general categories which are controlled drug release and modification to be used for purification of other substances. The controlled release of several drugs, including hydrophilic anticancer drugs, from poly(HEMA) nanoparticles has been documented (Chouhan and Bajpai 2009). Poly(HEMA) nanoparticles have been modified with an adsorbent in order to purify human serum albumin, antibodies, and deoxyribonucleic acid (Karakoc, Yılmaz, et al. 2009; Öztürk and Bereli 2008; Türkcan and Akgöl 2013). Nanoparticles were chosen as the delivery vehicle in an attempt to be less noticeable after administration.

2.4.2.1. Poly(HEMA) Nanoparticles

Free radical polymerization is the method used to produce poly(HEMA) (Chouhan and Bajpai 2009). More specifically, suspension and emulsion polymerization methods

are required to produce nano-sized polymer particles. Suspension polymerization is characterized by the use of a monomer soluble initiator and a monomer that are not soluble in the polymerization medium. The kinetics of the polymerization occurring in the suspension are similar to bulk polymerization or solution polymerization depending on the inclusion of an organic phase. Emulsion polymerization differs based on the use of an initiator that is soluble in the polymerization medium but not the monomer, as well as the use of an emulsifier in a high enough concentration to form micelles (Arshady 1992).

An example of a modified suspension method used to produce poly(HEMA) involves poly(vinyl alcohol) (PVA) as the stabilizer in the aqueous phase, ethylene glycol dimethacrylate (EGDMA) as the crosslinker, benzoyl peroxide (BPO) as the initiator, and toluene as the organic phase (Chouhan and Bajpai 2009). Surfactant free emulsion polymerization has also been used to produce poly(HEMA) which also used PVA and EGDMA as the stabilizer and crosslinker, respectively, as well as potassium persulfate as the initiator (Öztürk and Bereli 2008). The modified suspension method was used in other studies involving the poly(HEMA) nanoparticles (Gupta, Bajpai, et al. 2014). However, the latter method was found more frequently in the literature (Karakoc, Yılmaz, et al. 2009;Türkcan and Akgöl 2013; Uygun and Uygun 2014).

2.5. Polymer Degradation

2.5.1. Methods of Degradation in the Human Body

The three main components in the human body that are responsible for degradation of polymers are water, salts and enzymes. The body contains a large amount of water, approximately 60%, that is able to interact with materials in the body to

different extents based on their affinity. In general, the water content of a polymer ranges from 10^{-4} to 1 g/cm^3 (Deshayes and Kasko 2013; Zaikov 1985). Due to its high availability, water is the most common environmental trigger for polymer degradation. Degradation triggered by water, known as hydrolysis, occurs through chain scission as a result of a water molecule being added to the polymer backbone (Deshayes and Kasko 2013). Hydrolysis is a relatively fast degradation process that can be adjusted based on the molecular weight and monomeric unit selection (Acemoglu 2004).

The anions and cations from salts in solution, which impact the environmental acidity and alkalinity, may influence polymer degradation through hydrolysis and oxidation. Salts can diffuse into hydrophilic polymers at a rate similar to water and may have a catalytic effect on the hydrolytic breakdown of these polymers (Zaikov 1985). Oxidation is a relatively slow process that involves increasing a molecule's oxidation state. Oxidizing agents include reactive oxygen species, such as hydrogen peroxide, and reactive nitrogen species, such as nitric oxide (Acemoglu 2004; Deshayes and Kasko 2013).

Lysosome enzymes from macrophages can participate in polymer degradation by leaving the macrophage and interacting with the polymer surface or by remaining inside the macrophage and interacting with polymer fragments that have been ingested. Examples of lysosome enzymes include hydrolases and oxidases that can be involved in polymer degradation through hydrolysis and oxidation (Zaikov 1985).

Similar to oxidative environments, reductive environments also exist within the body. The presence of a reductive environment is often due to oxidative stress (Deshayes

and Kasko 2013). Several reducing agents are made by cells including glutathione, also known as GSH, which is a low molecular weight thiol found in high concentrations in biological systems (Deshayes and Kasko 2013; Meng, Hennink, et al. 2009). The concentration of GSH is relatively higher in the intracellular environment (0.5 to 10 mM) compared to the extracellular environment and in circulation (2 to 20 μM) (Meng, Hennink, et al. 2009). Polymer degradation by reduction occurs relatively quickly compared to hydrolytic degradation. Reductive degradation may occur within minutes to hours in highly reductive environments (Meng, Hennink, et al. 2009).

2.5.2. Synthesis of Degradable Polymers

Degradation of polymers is important because it promotes their removal in a safe and non-invasive manner (Deshayes and Kasko 2013). The chemical structure is the most significant factor that influences degradation because it dictates the stability of functional groups, chemical reactivity, affinity to water, and swelling behaviour of the polymer (Acemoglu 2004). The preferred type of degradable linkage and location within the polymer need to be taken into account when designing the chemical structure. The degradable linkage may be located in the polymer's backbone, side chains, crosslinks, or any combination of the previously listed locations. If the degradation occurs in the backbone, lower molecular weight fragments will be produced that are generally associated with a higher solubility. Degradation of the crosslinks results in lower molecular weight fragments compared with the original polymer. The solubility of these polymer chain fragments is likely to be different from the crosslinked polymer. Degradation of the side chains results in the removal of small fragments and potentially a

change in the solubility of the main polymer (Deshayes and Kasko 2013). The crosslinks were selected as the location for degradation for this work so that the main material for nanoparticle synthesis did not have to be altered

Previous research has determined that various polymers and materials can undergo each type of degradation mentioned in the previous section. This information can also be used to separate the classes of polymers into different groups based on their method of degradation. Types of polymers that are known to undergo degradation by hydrolysis include polyamides, polyanhydrides, polycarbonates, polyesters, polyphosphoesters, and polyurethanes. However, anhydride or ester bonds are commonly used because not all of these polymers degrade at the appropriate time scale under physiological conditions. The degradation of ester bonds occurs within a few weeks to months under physiological conditions (Deshayes and Kasko 2013). The issue with degradation of polyesters and polyanhydrides is that it can cause a local pH decrease that is detrimental to acid sensitive drugs (Acemoglu 2004). Types of polymers that are associated with oxidative degradation include polycarbamates, poly(ether urethane urea)s, polysulfides, and polyurethanes (Acemoglu 2004; Deshayes and Kasko 2013). Polysulfides are most commonly used because of their initial hydrophobic state, which is useful for carrying hydrophobic drugs, and transition to hydrophilic polysulfoxides/polysulfones, allowing them to be excreted through the renal system (Deshayes and Kasko 2013). Materials that undergo reductive degradation generally contain disulfide bonds (Meng, Hennink, et al. 2009). These disulfide bonds are cleaved by thiol-disulfide exchange reactions with thiols in the surrounding environment (Deshayes and Kasko 2013). BAC was selected as the

degradable crosslinker for this work because it is similar in structure to EGDMA, the original crosslinker selected.

2.6. Mucoadhesive Materials

2.6.1. Categories of Polymers

There are several categories of mucoadhesive materials such as cationic polymers, anionic polymers, non-ionic polymers, amphoteric polymers, and boronic acid copolymers (Khutoryanskiy 2011). Ionic polymers, cationic and anionic, have been previously found to be more mucoadhesive relative to non-ionic polymers (Khutoryanskiy 2011; Ludwig 2005). The potential reasoning for the mucoadhesive ability of cationic polymers is that the positive charges may take part in electrostatic interactions with the negative charges on mucosal surfaces (Khutoryanskiy 2011; Lehr, Bouwstra, et al. 1992; Smart 2005). This interaction is likely to be stronger in neutral and/or slightly alkaline medium, which means that the mucoadhesive property will also be stronger for cationic polymers under these conditions (Lehr, Bouwstra, et al. 1992). Chitosan, a cationic polymer, is involved in more complex mucoadhesive interactions including hydrogen bonding and hydrophobic effects along with the major mechanism, electrostatic interactions. However, the level of impact each interaction has on mucoadhesion is dependent on other factors such as pH and the presence of other chemicals (Khutoryanskiy 2011).

Anionic polymers display mucoadhesive ability because of their carboxyl groups which have the ability to form hydrogen bonds with hydroxyl groups present in the mucin layer (Khutoryanskiy 2011). However, the mucoadhesive property of an anionic polymer

is significantly decreased when there are multivalent cations, such as Ca^{2+}, Mg^{2+}, and Fe^{3+}, nearby due to precipitation and/or coagulation of the polymer. Additionally, as the pH of the environment increases so does the swelling of the polymer, which may lead to a decrease in mucoadhesion (Hombach and Bernkop-Schnürch 2010). Sodium alginate, an anionic polymer, does not owe its mucoadhesive behaviour solely to the presence of carboxyl end groups. The low surface tension of sodium alginate relative to the mucin coated cornea allows the polymer to spread over the cornea improving its mucoadhesive characteristic (Ludwig 2005). Additionally, the mucoadhesive performance of sodium alginate can be increased by increasing charge density (Khare, Grover, et al. 2014).

Quantifying the mucoadhesive property of non-ionic polymers has generally been unsuccessful due to the fact that the interactions between non-ionic polymers and mucin are weak. Non-ionic polymers may display mucoadhesive characteristics if they are able to diffuse into and form an interpenetration layer with the mucin layer (Khutoryanskiy 2011). It is also noted that after interpenetration of the non-ionic polymer in the mucin layer, the polymer chains should form entanglements. The mucoadhesive characteristic of non-ionic polymers does not depend on pH or electrolytes (Hombach and Bernkop-Schnürch 2010).

Amphoteric polymers, which contain both cationic and anionic functional groups, have only been included in a few mucoadhesion based studies (Khutoryanskiy 2011). Therefore, the knowledge of their mucoadhesive ability is limited. It is assumed that mucoadhesion of amphoteric polymers is minimal because of self-neutralization of the cationic and anionic groups present in the same macromolecule (Withers, Cook, et al.

2013). However, it is predicted that the mucoadhesive ability of these polymers is dependent on the solution pH and their isoelectric point due change in properties related to the shift between positive, neutral, and anionic states. For example, the viscosity of the polymer solution is minimized at the isoelectric pH relative to higher and lower pH values (Khutoryanskiy 2011). Even with minimal mucoadhesive ability, it is expected that amphoteric polymers are relatively more mucoadhesive compared to non-ionic polymers (Ludwig 2005).

Boronic acid copolymers have shown potential as a mucoadhesive material. Mucoadhesion occurs because of the interactions of boronic acids with the diols of sialic acids residues and other sugar residues of mucin (Zhang, Wang, et al. 2012). Multiple ester bonds are formed between the boronic acids and the diols of mucin (Ivanov, Solodukhina, et al. 2012). Studies have shown the formation of insoluble complexes between boronic acid copolymers and porcine mucin. These insoluble complexes could be dissolved when fructose was added to the solution because of the competition between mucin and fructose for the boronic acids. These polymers form the strongest complexes with mucin at pH values of 7 to 9 (Khutoryanskiy 2011). The Sheardown Lab Group is currently interested in the use of phenylboronic acid to create mucoadhesive materials.

2.6.2. Incorporation in Ophthalmic Nanoparticles

Mucoadhesive materials have been incorporated in a variety of different nanoparticles for delivery to the transmucosal routes to increase retention time (Ghate and Edelhauser 2006). Hyaluronic acid, an anionic mucoadhesive polymer, has been coated on polymer nanoparticles with the potential to be used for ocular drug delivery (Ibrahim

and El-Leithy 2010). Nanoparticles have also been modified with chitosan to make them mucoadhesive in a few studies (Bravo-Osuna and Vauthier 2007; Nagpal and Singh 2010). In one study involving both chitosan and hyaluronic acid, chitosan nanoparticles were further modified with hyaluronic acid to further improve their mucoadhesive ability (Wadhwa and Paliwal 2010).

3. MATERIALS AND METHODS

3.1. Materials

HEMA, EGDMA, inhibitor remover beads, methacrylic acid (MAA), sodium dodecyl sulfate (SDS), benzoyl peroxide (BPO), 1-butanol, dexamethasone, 3(acrylamido)phenylboronic acid, DTT, MTT reagent (3-(4,5-dimethylthiazol-2-yl)-2,5-diphenyl tetrazolium bromide), mucin from bovine submaxillary glands, and potassium bromide (KBr) were purchased from Sigma-Aldrich. BAC was purchased from Alfa Aesar and potassium chloride (KCl) was purchased from EMD chemicals.

Spectra/Por® 6 regenerated cellulose 50 kDa molecular weight cut off (MWCO) dialysis tubing were purchased from Spectrum® Laboratories. Acrodisc CR 13 mm high pressure liquid chromatography (HPLC) grade syringe filter with a 0.2 μm pore size were purchased from PALL Life Sciences.

3.2. Nanoparticle Preparation

3.2.1. Poly(HEMA) Nanoparticle Preparation

PolyHEMA nanoparticle suspensions were prepared as follows. HEMA and EGDMA were passed through a column packed with inhibitor remover beads. The components of the organic phase, 9.30 mmol of HEMA, 0.795 mmol of EGDMA, 0.504 mmol of MAA, 0.186 mmol BPO, and 1.5 ml of 1-butanol, were mixed together in a 20 ml scintillation vial until the BPO dissolved. Next, a 200 ml 0.06% w/v SDS solution was prepared in a 500 ml Erlenmeyer flask and a magnetic stir bar was added. The flask was then sealed and bubbled with N_2 gas for 40 minutes. The organic phase solution was added to the sealed flask. Next, the flask was placed in an oil bath on top of a heated stir

plate and mixed at 700 rpm at a temperature of 80°C for 2 hours. The temperature was increased to 90°C for 1 hour at which time the flask was removed from the heated oil bath and left to cool to room temperature. The chemical structures of all compounds previously mentioned can be found in Figure 2, with the exception of HEMA which is shown in its polymerized form in Figure 1.

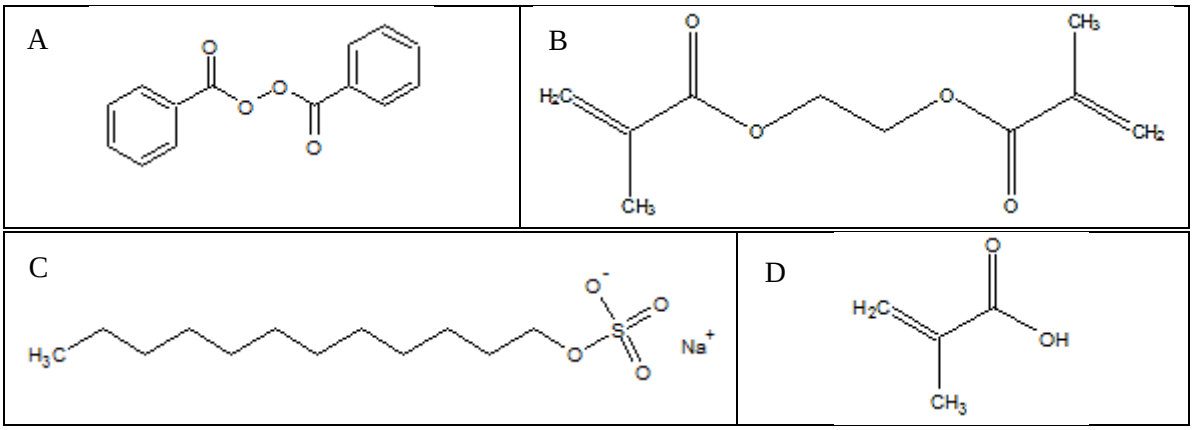

Figure 2. Chemical structures of BPO (A), EGDMA (B), SDS (C), and MAA (D).

3.2.2. Modifications to Preparation Method

Formulations containing BAC were made using a method similar to the one described in Section 3.2.1. The changes made to the method in Section 3.2.1 were the exclusion of EGDMA from the organic phase, the addition of 0.595 mmol of BAC to the organic phase, and the increase of 1-butanol from 1.5 ml to 4 ml.

Formulations containing 3AAPBA were made using a modified version of the method described in Section 3.2.1. The method in Section 3.2.1 was altered by the addition of 0.393 mmol of 3AAPBA to the organic phase.

Drug loaded formulations were prepared as described above with the addition of 18 mg of dexamethasone to the organic phase. The chemical structures of BAC and 3AAPBA can be found in Figure 3.

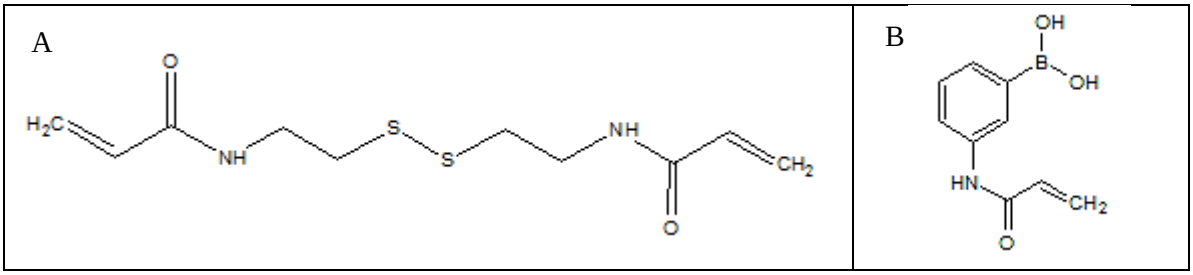

Figure 3. Chemical structures of BAC (A) and 3AAPBA (B).

3.2.3. Purification of Nanoparticle Suspension

To purify the nanoparticle suspensions, the cooled products were placed in Spectra/Por® 6 regenerated cellulose dialysis tubing with a MWCO of 50 kDa. The tubing was place in 4 L plastic containers filled with milliQ water. The milliQ water was changed 10 times over the course of 10 days. After 10 days the nanoparticle suspension was removed from the tubing, put in falcon tubes, and put in the freezer. Then, the frozen nanoparticle suspension was freeze dried.

3.3. Nanoparticle Characterization

3.3.1. Size Determination

The dynamic light scattering (DLS) function of the Brookhaven 90 Plus Particle Size Analyzer was used to obtain the average effective diameters of the nanoparticles. 1 ml of the nanoparticle sample was added to a polystyrene two clear sided cuvette. 2 to 4 ml of milliQ water were added to the cuvette in order to dilute the solution to obtain an acceptable level of transparency, which was determined by the suggested range for the

count rate. The sample in the cuvette was well mixed and then analyzed by the Brookhaven Size Analyzer.

3.3.2. Molecular Composition

The molecular structure of the nanoparticles was determined using Fourier Transform Infrared Spectroscopy (FTIR) with a Bruker Hyperion 3000 Microscope with a Vertex 70 Bench and HTS Plate Reader. Freeze dried poly(HEMA) nanoparticles crosslinked with EGDMA were analyzed using attenuated total reflectance FTIR (ATR-FTIR). Freeze dried poly(HEMA) nanoparticles co-polymerized with 3AAPBA and crosslinked with BAC were evenly dispersed in KBr powder. The mixture was packed into the well of a metal plate prior to analysis.

3.3.3. Morphology

TEM was used to observe the morphology of the nanoparticles. First, the nanoparticle suspensions were diluted by a factor of 5 to 10 with milliQ water after which 5 μL of the diluted suspension was added to a TEM grid for TEM analysis. Analysis was performed using a JEOL 1200EX TEMSCAN at a magnification of 25000.

3.3.4. Degradation

To evaluate the degradation of the materials the pH of milliQ water was adjusted to 8.5 using 0.1 M sodium hydroxide. A 20 mM DTT solution was made in a 10 ml sealed round bottom flask, with the pH adjusted milliQ water, and bubbled with N_2 gas for 10 minutes. 4 ml of the nanoparticle suspension, poly(HEMA) crosslinked with BAC, was added to two separate 10 ml round bottom flasks. 4 mL of pH 8.5 milliQ water was added to the first flask containing the nanoparticle suspension. 4 ml of the 20 mM DTT solution

was added to the second flask with the nanoparticle suspension. The solutions in both nanoparticle flasks were bubbled with N_2 gas for 10 minutes. The two nanoparticle flasks were then placed in a shaking incubator at 37°C for a minimum of five days.

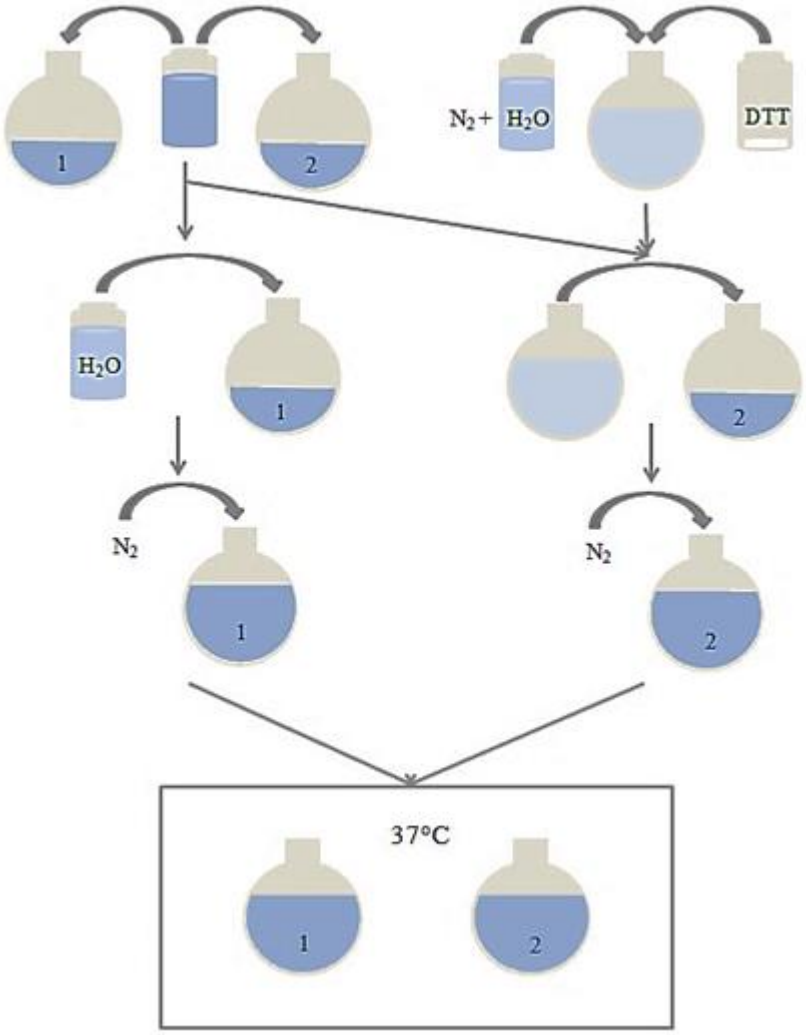

Figure 4. Schematic of method used for testing nanoparticle degradation.

300 μL of each solution was subsequently added to a Costar UV transparent 96 well plate. The absorbance values of the samples were obtained at a wavelength of 350 nm using a

Tecan M200 Infinite Pro plate reader. Each solution was also analyzed according to the method listed in Section 3.3.3 titled Morphology.

3.3.5. Mucoadhesion

The zeta potential function of the Brookhaven 90 Plus Particle Size Analyzer was used to assess the mucoadhesive properties of the nanoparticle formulations. 100 mM KCl and 4 mg/ml BSM stock solutions were prepared prior to zeta potential sample preparation. Test samples were prepared by adding 0.4 ml of a poly(HEMA, BAC, 3AABPA) nanoparticle sample or 0.1 ml of a poly(HEMA, BAC) sample, 0.2 ml of the BSM stock solution, and 0.5 ml of the KCl stock solution to a 2ml eppendorf, followed by diluting the sample to 2ml with milliQ water. Nanoparticle control samples were prepared in a similar manner to the test samples with the exception the 0.2 ml of BSM stock solution being replaced with milliQ water. Mucin control samples were also prepared in a similar manner to the test samples, however the nanoparticle sample volume was replaced with milliQ water. These samples were then placed in a shaking incubator at 37°C for 3 hours, at which time they were transferred to a cuvette and an AQ-1204 probe was inserted into the solution. The probe was then connected to the Brookhaven 90 Plus Particle Size Analyzer and the zeta potential of the samples was determined. A decrease in zeta potential should be observed when mucin adheres to the nanoparticle surface due to the negative zeta potential associated with mucin. In order to confirm mucoadhesion, the zeta potential of the nanoparticle samples incubated with mucin should be significantly more negative relative to the zeta potential of the mucin control and the relative nanoparticle control.

3.4. Drug Release Studies

To remove loosely entrapped drug prior to drug release, 25 mL of the drug loaded nanoparticle suspension was ultracentrifuged eight times with an increasing rotation speed between 10,000 rpm and 20,000 rpm. The pellet was removed and placed in a glass vial after each centrifugation step. The collection of pellets were then resuspended in 25 ml of milliQ water by sonication using misonix S-4000 sonicator with an intensity of 40 for 15 minutes. The resuspended drug loaded nanoparticles were then put into Spectra/Por® 6 regenerated cellulose dialysis tubing with a 50 kDa MWCO. The dialysis tube was then placed in a tube with 25 ml of milliQ water, maintained at a temperature of 34°C and shaken continuously. The entire volume of water surrounding the dialysis tubing was removed and replaced at specified intervals to obtain drug release measurements and to ensure sink conditions. The collected samples were filtered using HPLC grade Acrodisc CR 13 mm syringe filters with a pore size of 0.2 μm. The filtered samples were analyzed using HPLC with a water/acetonitrile (60/40, v/v) mobile phase flowing at 1 ml/min, an Atlantis dC18 5 μm (6x100 mm) column, a Waters 1525 Binary HPLC pump, a Waters 2707 Autosampler, and a Waters UV/Visible Detector set to a wavelength of 254 nm. The first 60% of the drug release curves were analyzed using the Korsmeyer-Peppas model (Equation 1)

$$\frac{M_t}{M_\infty} = Kt^n \tag{1}$$

where t is the time selected, M_t and M_∞ are the mass released at time t and the amount of drug loaded respectively, K is the rate constant, and n is the release exponent (Singhvi and Singh 2011). K and n were found using Equations 2 and 3 (Weisstein 2002)

$$n = \frac{N\sum_{i=1}^{N}\left(ln\ t_i \times ln\left(\frac{M_t}{M_\infty}\right)_i\right) - \sum_{i=1}^{N}(ln\ t_i)\times\sum_{i=1}^{N}\left(ln\left(\frac{M_t}{M_\infty}\right)_i\right)}{N\sum_{i=1}^{N}(ln\ t_i)^2 - \left(\sum_{i=1}^{N} ln\ t_i\right)^2} \quad (2)$$

$$K = exp\left(\frac{\sum_{i=1}^{N}\left(ln\left(\frac{M_t}{M_\infty}\right)_i\right) - n\sum_{i=1}^{N}(ln\ t_i)}{N}\right) \quad (3)$$

where i refers to each drug release measurement and N is the total number of measurements used to calculate the coefficients. These equations were obtained using the least squares fitting technique (Weisstein 2002). The release exponent and release constant are used to make assumptions regarding the drug release mechanism and the structural/geometric characteristics of the polymeric system, respectively (Siepmann and Siepmann 2008). After eight weeks it was assumed that the entire amount of drug loaded had been released from the nanoparticles. Therefore, drug loading was determined by measuring the amount of drug that was released after eight weeks.

3.5. Cell Viability Studies

The viability of HCEC in the presence of the nanoparticle suspensions was determined with an MTT assay. HCEC (10,000/well) and 200 µl of keratinocyte serum free medium (KSFM) were added to the wells of a 96-well microtiter plate (Grenier). The plate was then stored in the incubator at 37°C and 5% CO_2 for a minimum of 3 hours. Next, 50 µl of the nanoparticle suspensions, at original and reduced concentrations, were added to the wells containing HCEC. Then, the well plate was placed back in the incubator at 37°C and 5% CO_2 for 2 days. After 2 days, the media and nanoparticle suspensions were removed from the well plate, followed by the addition of 100 µl of KSFM and 10µl of MTT reagent (3-(4,5-dimethylthiazol-2-yl)-2,5-diphenyl tetrazolium

bromide) solution, at a concentration of 5 mg/ml in phosphate buffered saline (PBS), to each well. The cells were incubated with the MTT reagent at 37°C and 5% CO_2 for 2 hours. During this incubation period the water soluble MTT reagent was cleaved by intracellular succinate dehydrogenase resulting in formazan. Formazan is purple, insoluble, and unable to permeate through the membranes of healthy cells (Fotakis and Timbrell 2006). Then, the MTT reagent and media was removed and replaced with 50 µl of dimethyl sulfoxide (DMSO), which is used to dissolve the formazan crystals. Finally, the amount of formazan in each well was obtained by measuring the absorbance at a wavelength of 540 nm using a Tecan M200 Infinite Pro plate reader. The cell viability (%) relative to the controls which contained HCEC without nanoparticles was determined by Equation 4

$$Cell\ Viability\ (\%) = \frac{[A]_{test}}{[A]_{control}} \times 100\% \quad (4)$$

where $[A]_{test}$ and $[A]_{control}$ are the absorbance of the test well and the control well, respectively.

3.6. Statistical Analysis

In order to determine the significance of the results for the turbidity test for degradation, zeta potential test for mucoadhesion, and cell viability studies, p values were obtained using paired t-tests. This method was selected because of the small sample sizes.

4. RESULTS AND DISCUSSION

4.1. Nanoparticle Characterization

4.1.1. Size Determination

Poly(HEMA) nanoparticles, prepared according to section 3.2.1, were analyzed using DLS to determine the average effective diameter (Table 1). The diameters listed in the table are within the range of 97.8 nm to 125.5 nm. This range of diameters does not exceed the maximum of 200 nm specified in the objectives. Therefore all formulations meet the size objective.

Table 1. Average effective diameter and polydispersity of poly(HEMA) nanoparticles crosslinked with EGDMA. Nanoparticle formulations contained various amounts of organic phase, surfactant, and monomer phase. The error associated with the diameter and polydispersity was obtained from the standard deviation of minimum triplicate measurements.

Sample	**A1**	**A2**	**A3**	**A4**	**A5**	**A6**	**A7**	**A8**
Monomer	0.75X				1X			
SDS (mg)	119		159		119		159	
1-butanol (ml)	1.5	2.0	1.5	2.0	1.5	2.0	1.5	2.0
Average Effective Diameter (nm)	107.5 ± 0.5	115.5 ± 0.9	97.8 ± 0.3	105.9 ± 0.5	125.5 ± 0.9	123.3 ± 0.9	119.6 ± 1.4	118.4 ± 0.7
Poly-dispersity	0.032 ± 0.010	0.048 ± 0.009	0.031 ± 0.017	0.042 ± 0.029	0.063 ± 0.014	0.043 ± 0.021	0.054 ± 0.017	0.053 ± 0.028

The equation obtained by creating a linear model using the statistical software R can be found in Equation 5 where x_A, x_B, x_C, all refer to coded variables of -1 and +1 corresponding to the low and high value for their respective parameters, 1-butanol (A), SDS (B), and monomer (C), listed in Table 1 and y refers to the nanoparticle diameter.

$$y = 114.19 + 1.59x_A - 3.76x_B + 7.51x_C + 0.13x_Ax_B - 2.44x_Ax_C + 1.06x_Bx_C \quad (5)$$

The three factors that have the strongest influence on the nanoparticle diameter are the amount of SDS ($p<0.01$), amount of monomer ($p<0.001$), and the interaction between the amount of 1-butanol and monomer ($p<0.01$). Equation 5 predicts that the nanoparticle diameter will decrease with increased SDS and decreased monomer within the ranges studied. Additionally, this equation predicts that the nanoparticle diameter will decrease if the amount of 1-butanol and monomer are at the same level (159 mg SDS and 1X monomer or 119mg SDS and 0.75X monomer). Due to the fact that the monomer amount has the highest impact on the nanoparticle diameter, it was held constant at 0.75X for the rest of the formulations. The polydispersity values, determined from DLS, did not appear to follow any trend and were all within the range of 0.031 to 0.063.

Poly(HEMA, BAC) nanoparticles prepared according to section 3.2.1 with the modifications listed in section 3.2.2 were analyzed using DLS to determine the average effective diameter values included in Table 2. The diameters listed in the table are within the range of 227.0 nm to 302.6 nm.

Table 2. Average effective diameter and polydispersity of poly(HEMA) nanoparticles crosslinked with BAC. Nanoparticle formulations contained various amounts of organic phase, surfactant, and crosslinker. The monomer phase amount was kept constant at 0.75X. The error associated with the diameter and polydispersity was obtained from the standard deviation of triplicate measurements.

Sample	**B1**	**B2**	**B3**	**B4**
BAC (mg)	207	207	207	155
1-butanol (ml)	2.5	4	4	4
SDS (mg)	159	159	119	119
Average effective diameter (nm)	302.6 ± 2.4	262.9 ± 0.7	227.0 ± 2.9	229.7 ± 1.7
Polydispersity	0.266 ± 0.007	0.176 ± 0.016	0.228 ± 0.010	0.047 ± 0.016

Not all of the parameters varied for the formulations listed in Table 1 were repeated for the formulations listed in Table 2. The amount of 1-butanol was increased to allow more of the crosslinker to dissolve prior to polymerization. Even though the two greatest factors for altering the size were the amount of SDS and monomer, only the SDS was modified. This is because decreasing the monomer amount further would result in very small yields when freeze drying the particles, whereas changing the SDS amount was found to not have a large impact on the yield. The amount of BAC was originally selected to match the molar amount of EGDMA used in the first set of formulations. However, the amount of BAC was reduced for formulation B4 in an effort to reduce costs. The diameters from Table 2 do not meet the size objective set for this project because they exceed the maximum of 200 nm. However, optimization was not performed at this stage due to the fact that the nanoparticles still required further modification to add a mucoadhesive component. The two samples with the smallest diameter in Table 2 are samples B3 and B4, which are similar in size. However, the main difference between these two samples is that sample B4 has a relatively smaller polydispersity. Therefore, the amount of BAC was held constant at 155 mg for the remaining nanoparticle formulations.

Poly(HEMA, BAC, 3AAPBA) nanoparticles prepared according to section 3.2.1 with the modifications listed in section 3.2.2 were analyzed using DLS to determine the average effective diameter. The results are shown in Table 3. The amount of 3AAPBA was varied to determine its impact on the mucoadhesive behaviour of the nanoparticles. The diameters listed in the table are within the range of 179.5 nm to 219.4 nm. Samples

C2, C3, C4, and C5 met the size objective, whereas samples C1 and C6 did not. However, the diameters of the latter samples only exceed 200 nm by approximately 4 nm to 20 nm.

Table 3. Average effective diameter and polydispersity of poly(HEMA) nanoparticles crosslinked with BAC and copolymerized with 3AAPBA. Nanoparticle formulations contained various amounts of 3AAPBA. The monomer phase amount was kept constant at 0.75X and the BAC amount at 155 mg. The error associated with the diameter and polydispersity was obtained from the standard deviation of triplicate measurements.

Sample	**C1**	**C2**	**C3**	**C4**	**C5**	**C6**
3AAPBA (mg)	25	50	75	100	125	150
Average effective diameter (nm)	219.4 ± 1.0	189.1 ± 1.6	183.8 ± 1.2	179.5 ± 1.2	182.8 ± 1.0	203.6 ± 1.6
Poly-Dispersity	0.093 ± 0.017	0.057 ± 0.017	0.054 ± 0.017	0.078 ± 0.017	0.086 ± 0.028	0.046 ± 0.028

Overall, all nanoparticle formulations synthesized had an average effective diameter of less than 303 nm.

4.1.2. Molecular Composition

The molecular composition of the nanoparticles was determined using ATR-FTIR in order to confirm that they are composed of poly(HEMA). The FTIR spectrum found for freeze dried poly(HEMA) nanoparticles, produced according to the method stated in Section 3.2.1, is shown in Figure 5. Figure 5 confirms that HEMA was polymerized to produce poly(HEMA) based on the peaks at the wavenumbers listed in Table 4.

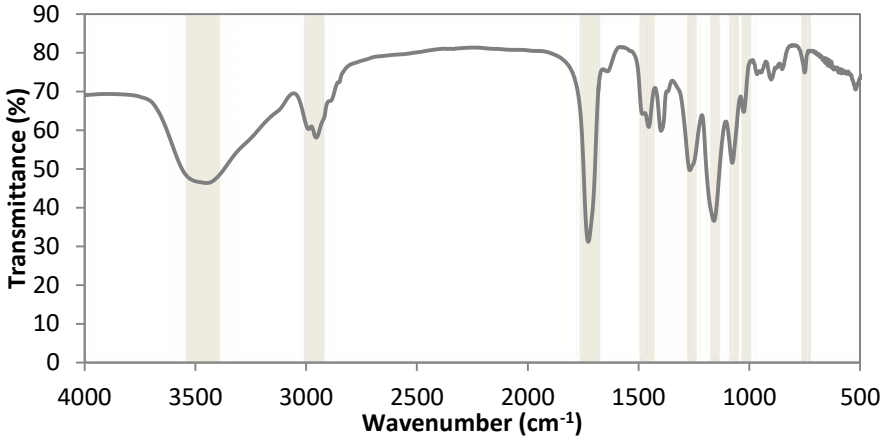

Figure 5. FTIR spectrum of poly(HEMA) nanoparticles crosslinked with EGDMA. The sample used to obtain the image was prepared according to the formulation listed for sample A1 in Table 1.

The peak assignments in Table 4 were obtained from previous literature involving characterization of poly(HEMA) (Perova, Vij, et al. 1997; Ferreira, Vidal, et al. 2000).

Table 4. Assignments for peaks at specified wavenumbers included in Figure 5.

Wavenumber (cm^{-1})	**Assignment**
3400-3500	OH stretching
2950	CH_2, CH_3 stretching
1720	C=O
1450-1500	CH_2 bending
1260	C-O stretching
1162	CH_3 rocking, OH torsion
1074	O-C stretching (alcohol group)
1021	C-O stretching (ester group)
750	O=C-O stretching

FTIR was also used to analyze poly(HEMA, BAC, 3AAPBA) nanoparticles in order to confirm the presence of 3AAPBA. It is assumed that the peak observed in Figure 6 around 650 cm^{-1} to 700 cm^{-1} corresponds to the out of plane C-H bending from the aromatic carbon ring because it falls within the range presented in the literature, which is 600 cm^{-1} to 900 cm^{-1} (Hudgins and Allamandola 1995). This peak is present in 3AAPBA,

and poly(HEMA, BAC, 3AAPBA) NP samples C1, C2, C3, C4, C5, and C6 from Table 3 but not in the poly(HEMA, BAC) NP sample B2 from Table 2. These results were expected because in the poly(HEMA, BAC) NP sample B2 there are no aromatic rings. However, there should be aromatic rings present in the poly(HEMA, BAC, 3AAPBA) samples if 3AAPBA was successfully integrated into the nanoparticles.

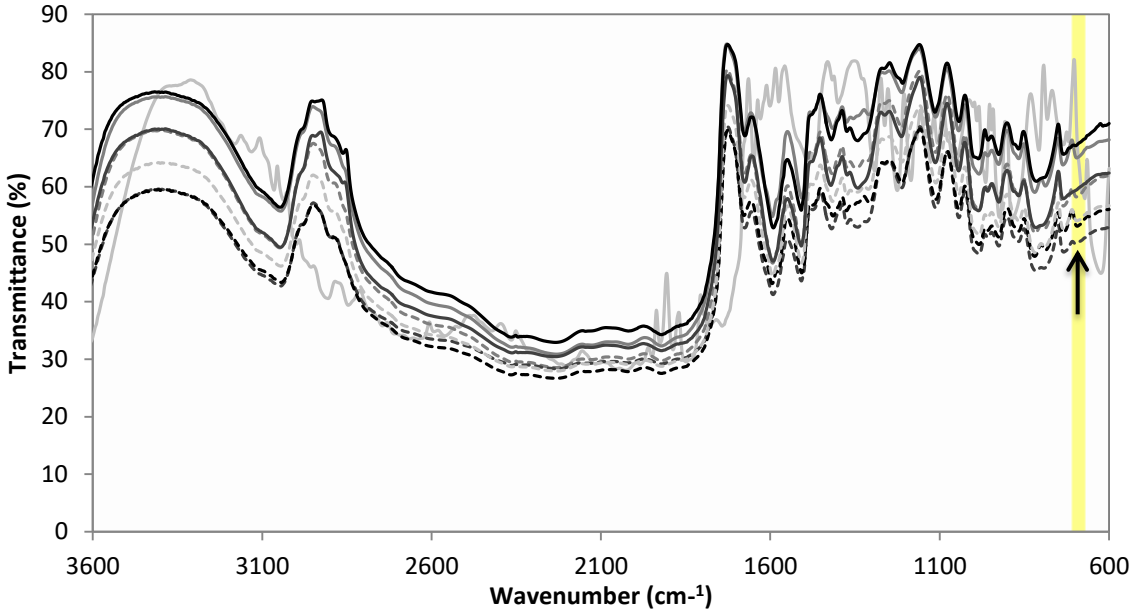

Figure 6. FTIR spectrum of 3AAPBA (—), poly(HEMA, BAC) nanoparticle sample B2 (▬) from Table 2, and poly(HEMA, BAC, 3AAPBA) NP samples C1 (▬), C2 (---), C3 (---), C4 (---), C5 (▬), and C6 (---) from Table 3. Samples were dispersed in KBr powder prior to analysis.

4.1.3. Morphology & Degradation

The morphology of dried poly(HEMA) nanoparticles, prepared according to Section 3.2.1 using the formulation from sample A2 in Table 1, can be observed in the TEM image included in Figure 7. The TEM image shows that spherical nano-sized particles were successfully synthesized.

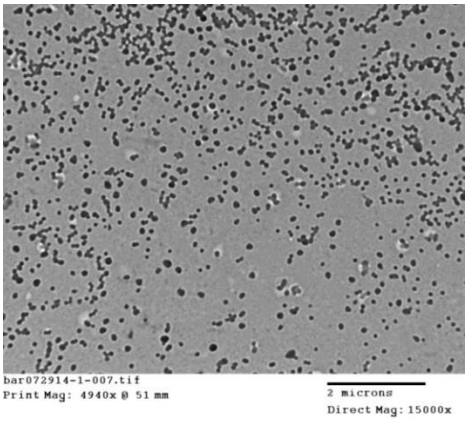

Figure 7. TEM image of poly(HEMA) nanoparticles, crosslinked with EGDMA, synthesized by suspension polymerization. The nanoparticles in the image were prepared according to the formulation listed for sample A8 in Table 1. Magnification of the image is 15000X.

Poly(HEMA, BAC) nanoparticles, prepared according to sections 3.2.1 and 3.2.2, with the formulation listed in sample B3 from Table 2, and poly(HEMA, BAC, 3AAPBA) nanoparticles, prepared according to sections 3.2.1 and 3.2.2 with various amounts of 3AAPBA, were observed with TEM as shown in Figures 8A, 9A, and 9C. Once again, spherical nano-sized particles were successfully synthesized.

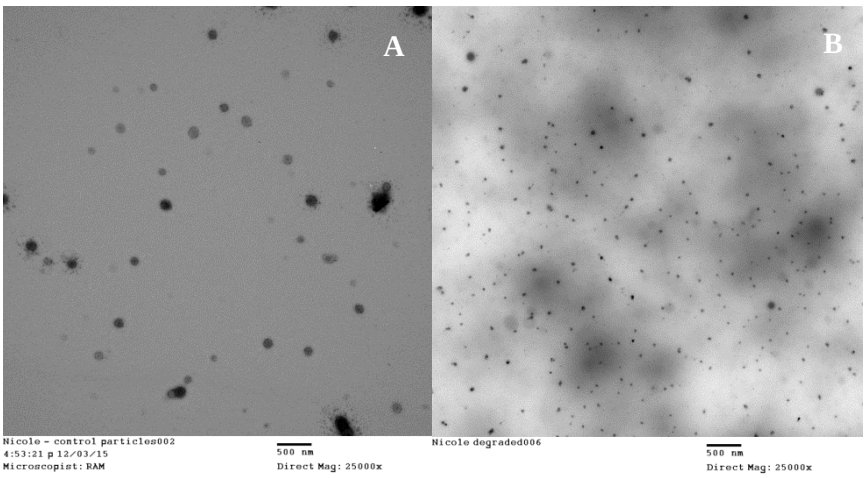

Figure 8. TEM images of samples after shaking incubation at 37°C for 5 days. Samples shown are poly(HEMA, BAC) nanoparticles, sample B3 from Table 2, with milliQ water (A) and with 10 mM DTT solution (B). For preparation the samples were diluted 10x and 5 μL was added to the TEM grid. The magnification of both images is 25000X.

The poly(HEMA, BAC) nanoparticles and poly(HEMA, BAC, 3AAPBA) nanoparticles were incubated with DTT to show their response to a reductive environment. The predicted reaction between the crosslinker used in the nanoparticles, BAC, and the reducing agent, DTT, is shown in Figure 10. TEM images of the nanoparticles incubated with DTT for 5 days were obtained in order to provide a comparison to their original shape and size. The TEM images of the nanoparticles after incubation with DTT can be found in Figures 8B, 9B, and 9D.

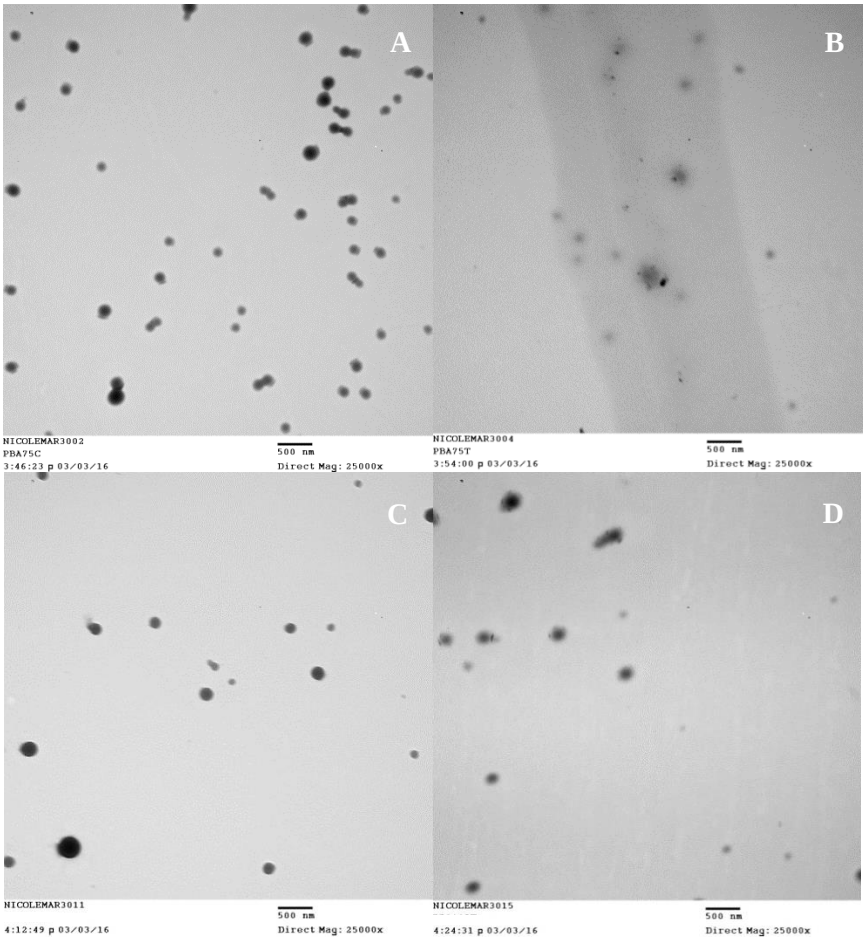

Figure 9. TEM images of samples after shaking incubation at 37°C for 5 days. Samples shown are poly(HEMA, BAC, 3AAPBA) nanoparticles, sample C3 and C6 in Table 3, in the presence of water (A,C) and 10 mM DTT (B,D), respectively For preparation the samples were diluted 5x and 5 μL was added to the TEM grid. The magnification of all images is 25000X.

It is evident based on Figure 9 that the poly(HEMA, BAC) nanoparticles decreased in size after incubation with DTT presumably because the dithiol bonds in the crosslinker were cleaved. The fragments observed in Figure 8B also appear to be less uniform, implying that the nanoparticles are being degraded. Similar observations can be found for poly(HEMA, BAC, 3AAPBA) nanoparticles shown in Figure 9B. The poly(HEMA, BAC, 3AAPBA) nanoparticles shown in Figure 9D are lighter relative to the same nanoparticles without DTT shown in Figure 9C. Additionally, darker randomly shaped spots can be seen near the edges of the lighter nanoparticles. These observations, although different than the ones obtained from the previous samples, support the theory that the nanoparticles degrade in the presence of DTT.

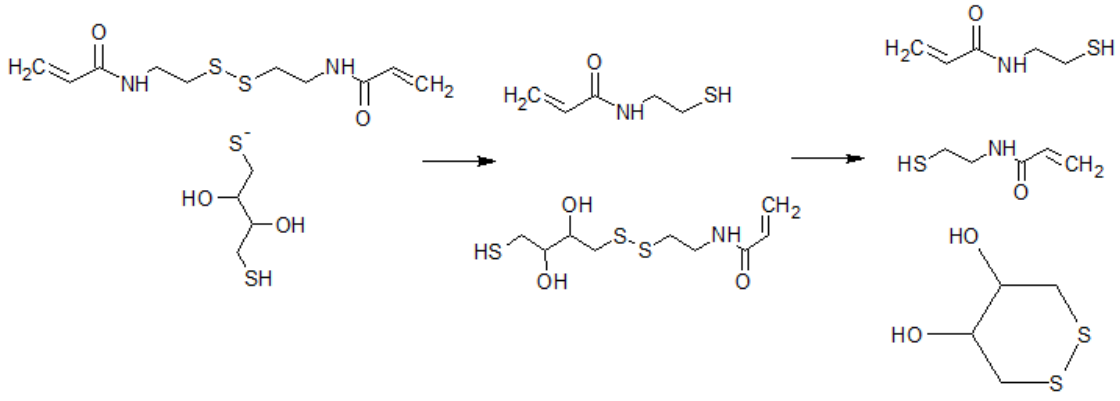

Figure 10. Cleavage of BAC through disulfide bond reduction in the presence of DTT.

Further confirmation of nanoparticle degradation in the presence of DTT was obtained using turbidity. The turbidity of each of the control and test solutions, prepared according to section 3.3.4, was determined indirectly by measuring the absorbance of each sample at 350 nm. As shown in Figure 11, the absorbance, and therefore the

turbidity, decreased for every poly(HEMA, BAC, 3AAPBA) nanoparticle formulation after incubation with DTT as expected. This further confirms the observations from the TEM images included in Figure 9.

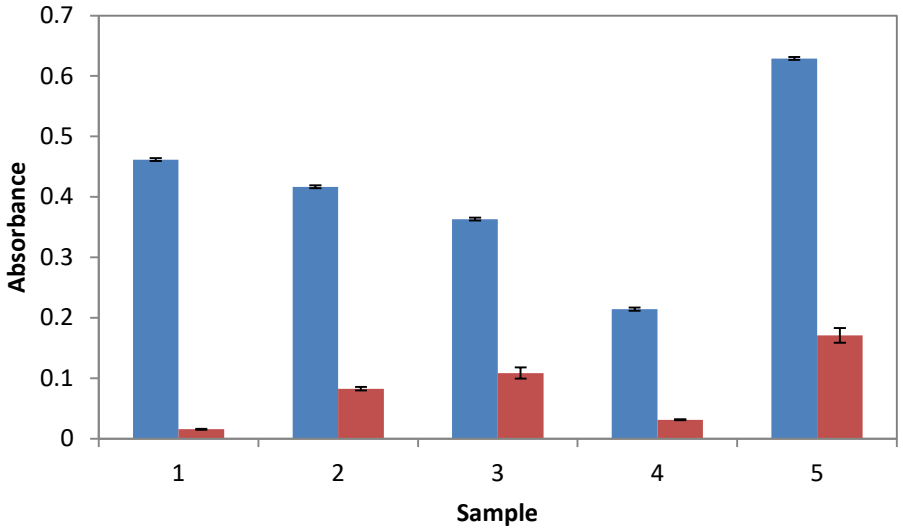

Figure 11. Absorbance readings at 350 nm of pHEMA (BAC, 3AAPBA) nanoparticles in the presence of water (■) and 10 mM DTT (■). Sample numbers correspond to samples C1 (1), C2 (2), C3 (3), C4 (4), and C5 (5) from Table 3. Error bars were obtained from standard error of 9 control samples and 27 test samples. For all samples $p < 0.0001$.

4.1.4. Mucoadhesion

Zeta potential values obtained from the mucin control, poly(HEMA, BAC) sample C4 from Table 2, and poly(HEMA, BAC, 3AAPBA) samples C2-C6 from Table 3 with and without mucin are shown in Figure 12. The mucin control shows that mucin has a negative zeta potential, as expected. The zeta potential of nanoparticles with mucin adsorbed to their surface is expected to decrease relative to the zeta potential of the nanoparticles without mucin.

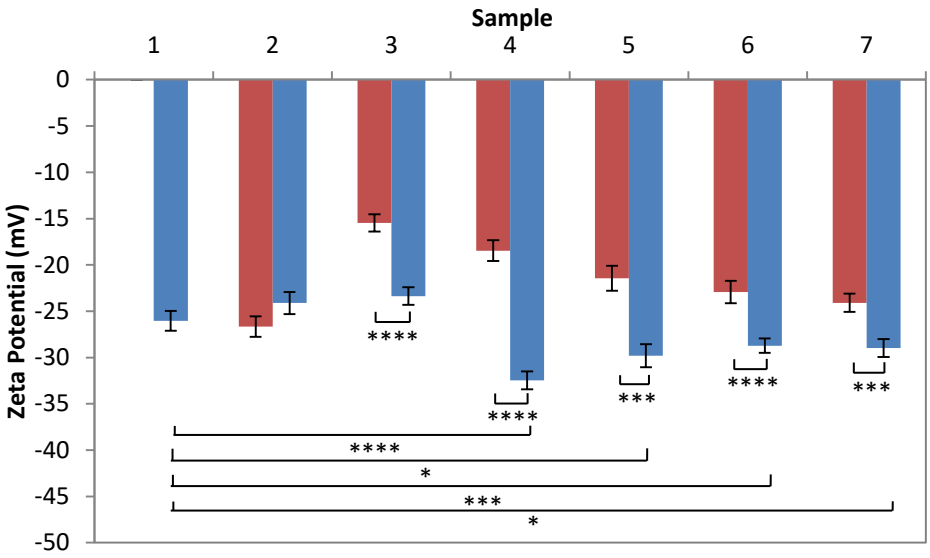

Figure 12. Zeta potential values of a mucin control solution (1), poly(HEMA, BAC) sample B4 from Table 2, and poly(HEMA, BAC, 3AAPBA) samples C2 (3), C3 (4), C4 (5), C5 (6), and C6 (7) from Table 3 with mucin (■) and without mucin (■). Error bars represent the standard error of 15 measurements. P value < 0.05 (*), <0.005 (***), and <0.0001 (****).

The zeta potential of poly(HEMA, BAC, 3AAPBA) sample C2 from Table 3 incubated with mucin was found to be signficantly lower than its corresponding nanoparticle control but not the mucin control. It is assumed that test samples with zeta potential values that are more negative than the relative control samples but less negative or the same as than the mucin control are assumed to not be mucoadhesive. This is because the decrease in zeta potential may be due to the addition of mucin to the sample and not interactions between the nanoparticles and mucin. There was no significant relationship found between the zeta potential of the poly(HEMA, BAC) sample B2 from Table 2 incubated with mucin and its corresponding nanoparticle control or the mucin control. Test samples with zeta potential values that are not significantly different from the corresponding

controls and the mucin control are also considered to not be mucoadhesive. The zeta potentials of the poly(HEMA, BAC, 3AAPBA) samples C3-C6 from Table 3 incubated with mucin were found to be signficantly lower than their corresponding nanoparticle control and the mucin control. Test samples with zeta potential values more negative than the mucin control were assumed to be mucoadhesive. In this case, the decrease in zeta potential cannot be explained by the mixture of mucin with the nanoparticles instead of interactions between the two solutes. Therefore, it is assumed that a zeta potential significantly lower than the mucin control and the corresponding nanoparticle sample is due to interactions between the nanoparticles and mucin.

4.2. Drug Release Studies

The release of dexamethasone from the poly(HEMA) nanoparticle formulation A3 from Table 1 and poly(HEMA, BAC, 3AAPBA) nanoparticle formulation C3 from Table 3, was measured over the course of seven days. This time period was selected because it is highly probable that the nanoparticles would not remain at the front of the eye for more than seven days based on an estimated mucosal turnover rate of 12 to 24 hours (Schäfer-Korting 2010). Figure 13 shows the dexamethasone release profile from poly(HEMA) nanoparticles. From this release curve, a rate constant of 0.001 and a release exponent of 0.607 were obtained. According to the literature, a release exponent value within the range of 0.43 to 0.85 from a spherical polymeric controlled delivery system corresponds to a drug release mechanism dictated by anomalous transport. This means that various types of phenomena, including diffusion and polymer swelling, may be contributing to the release of drug from the polymer spheres (Siepmann and Siepmann 2008).

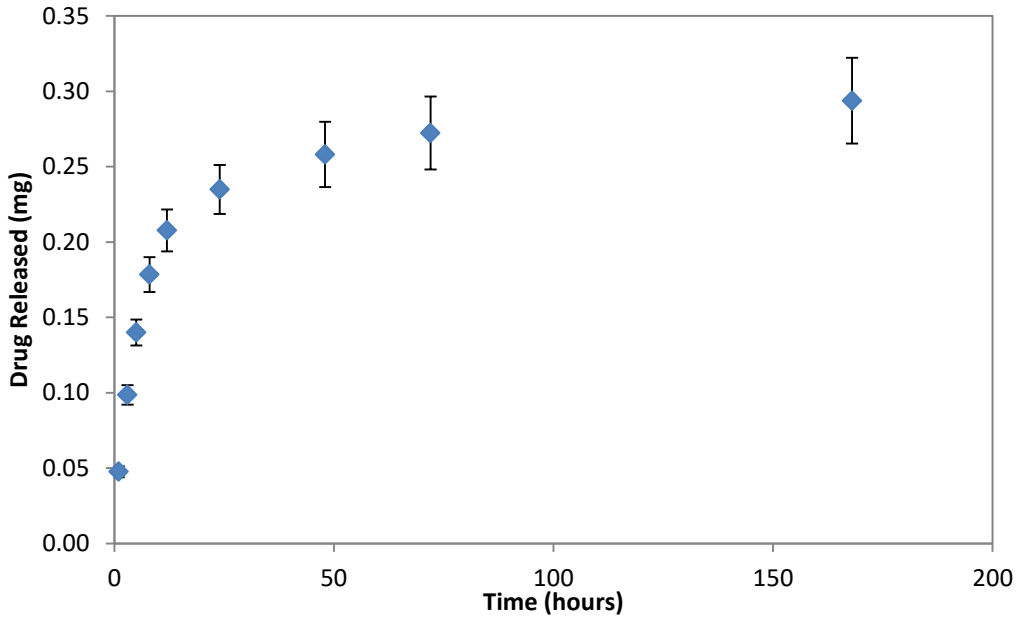

Figure 13. Dexamethasone release curve from loaded poly(HEMA) nanoparticles prepared according to sample A3 in Table 1 released from 50 kDa MWCO dialysis tubing under sink conditions. Initial loading of dexamethasone is 15.0% (±1.4%). Error bars were determined from standard error and error propagation.

Figure 14 shows the dexamethasone release profile from poly(HEMA, BAC, 3AAPBA) nanoparticles. It is important to note that the coefficients associated with the release curve in Figure 14 were calculated in a slightly different manner than stated in the method Section 3.4. The final amount of drug released was significantly higher than the amount released after one week. Therefore, it is suspected that there might be a two stage release of dexamethasone from these poly(HEMA, BAC, 3AAPBA) nanoparticles. Due to the fact that the Korsmeyer-Peppas model is based on the first 60% of the drug release, which is supposed to be the linear region, the calculations would not make sense using the actual value obtained for M_∞. Instead, M_∞ was selected as the amount of drug released after 144 hours. The rate constant and release exponent obtained from release curve in the previously mentioned figure are 0.002 and 0.586, respectively. This release exponent

corresponds to a drug release mechanism dictated by anomalous transport (Siepmann and Siepmann 2008).

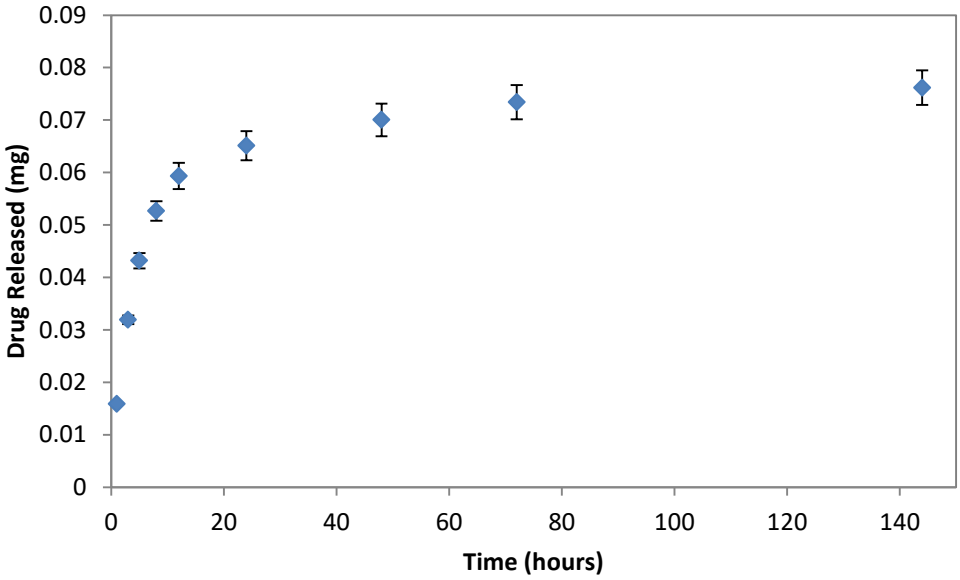

Figure 14. Dexamethasone release curve from loaded poly(HEMA, BAC, 3AAPBA) nanoparticles prepared according to sample C3 in Table 3 released from 50 kDa MWCO dialysis tubing under sink conditions. Initial loading of dexamethasone is 5.3% (±0.4%). Error bars were determined from standard error and error propagation.

The percentage of dexamethasone loaded in the nanoparticles is lower for the poly(HEMA, BAC, 3AAPBA) nanoparticles relative to the poly(HEMA) nanoparticles. A potential reason for this is that the mass percentage of the poly(HEMA) suspensions is greater or equal to three times the mass percentage of the poly(HEMA, BAC, 3AAPBA) suspensions. Additionally, the release exponents obtained from both release curves are very similar, with only a 3.5% difference relative to the release exponent from the data in Figure 13. This means that the drug release mechanism from both formulations of nanoparticles may be similar as well. Unlike the release exponents, the release constant

obtained from the data in Figure 14 was twice the value of the release constant obtained from the data in Figure 13. Therefore, it is suspected that there are differences in the structural characteristics of the two previously mentioned nanoparticle formulations.

4.3. Cell Viability Studies

The cytoxicity of the nanoparticle suspensions was tested using an MTT assay. The nanoparticle formulations examined were poly(HEMA) sample A1 from Table 1, poly(HEMA, BAC) sample B4 from Table 2, and poly(HEMA, BAC, 3AAPBA) samples C2 to C6 from Table 3. The poly(HEMA) and poly(HEMA, BAC) nanoparticles were tested at four different concentrations that include no dilution, 2x dilution, 4x dilution, and 8x dilution. The poly(HEMA, BAC, 3AAPBA) nanoparticles were only tested at two different concentrations, no dilution and 2x dilution, because the original suspensions are approximately 4x as dilute in comparison to the poly(HEMA) an poly(HEMA, BAC) nanoparticle suspensions. The results from the first MTT assay, shown in Figure 15, show that the HCEC viability is 88.5% to 182.5% after incubation with poly(HEMA) and poly(HEMA, BAC) nanoparticles. Based on the results obtained there does not appear to be a significant relationship between HCEC viability and the concentration of the poly(HEMA) and poly(HEMA, BAC) nanoparticles. Additionally, the HCEC viability was significantly higher for the poly(HEMA) nanoparticles relative to the poly(HEMA, BAC) nanoparticles with a dilution factor of 0 and 2 but not for a dilution factor of 4 and 8.

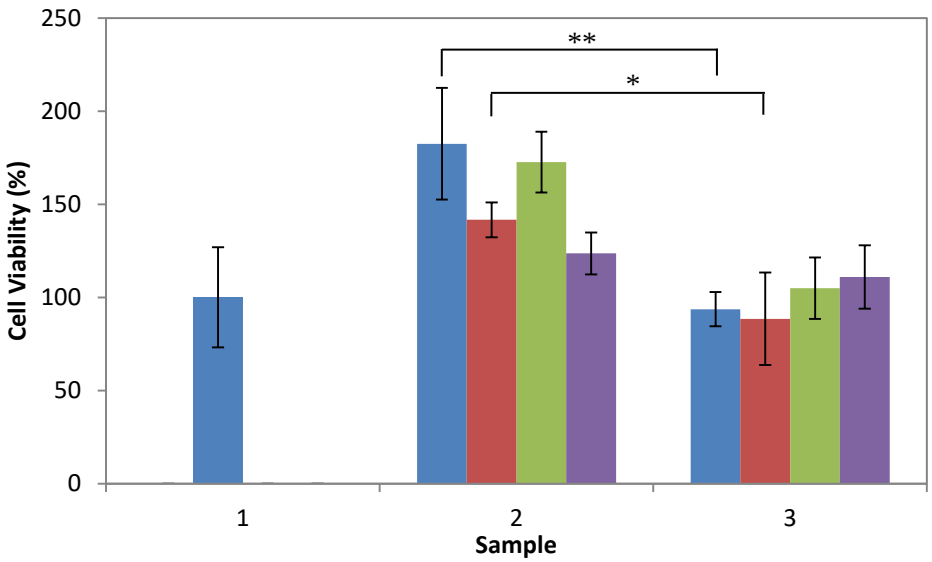

Figure 15. Cell viability of HCEC after incubation with poly(HEMA) and poly(HEMA, BAC) nanoparticles for 2 days at 37°C and 5% CO2. Samples shown are the control with no nanoparticles (1), poly(HEMA) nanoparticle formulation A1 (2) from Table 1, and poly(HEMA, BAC) nanoparticle formulation B4 (3) from Table 2. The bars correspond to original concentration (■), 2x dilution (■), 4x dilution (■), and 8x dilution (■). Error bars represent the standard error of triplicate samples. P value < 0.05 (*) and < 0.025 (**).

The results from the second MTT assay, included in Figure 16, show that the HCEC viability is 69.8% to 85.1% after incubation with poly(HEMA, BAC, 3AAPBA) nanoparticles. Based on the results obtained there does not appear to be a significant relationship between HCEC viability and the concentration of the poly(HEMA, BAC, 3AAPBA) nanoparticles. Additionally, there does not appear to be a significant relationship between HCEC viability and the different poly(HEMA, BAC, 3AAPBA) formulations tested, with the exception of sample 6 which has a significant relationship with samples 2 and 3. The HCEC viability was significantly lower after incubation with sample 6 compared to samples 2 and 3.

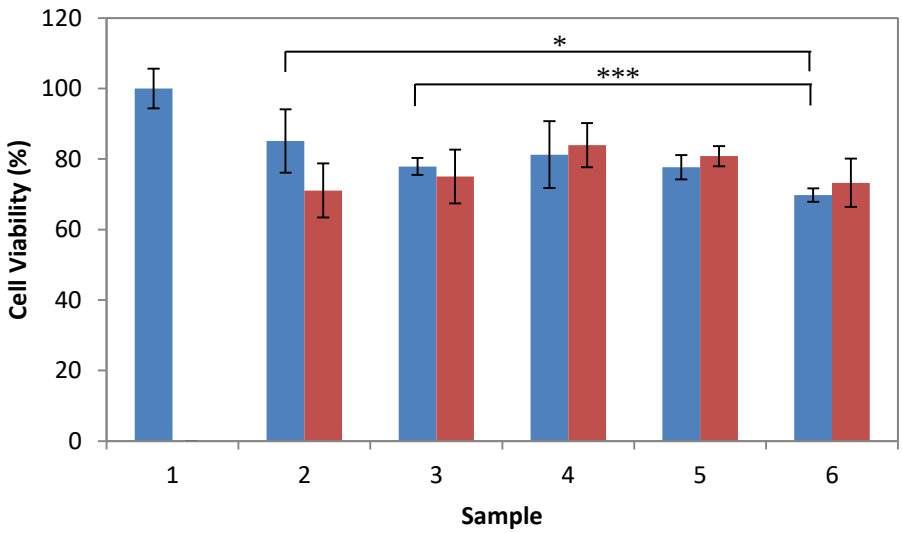

Figure 16. Cell viability of HCEC after incubation with poly(HEMA, BAC, 3AAPBA) nanoparticles for 2 days at 37°C and 5% CO2. Samples shown are the control with no nanoparticles (1) and poly(HEMA, BAC, 3AAPBA) nanoparticle formulation C2 (2), C3 (3), C4 (4), C5 (5), and C6 (6) from Table 3. The bars correspond to original concentration (■) for all samples and 2x dilution (■). Error bars were obtained from the standard error of triplicate samples. P value < 0.05 (*) and <0.005 (***).

Overall, these results show that the nanoparticles tested did not have an serious impact on the HCEC viability.

5. CONCLUSIONS

In conclusion, poly(HEMA) based nanoparticles that have the potential to serve as an ophthalmic drug delivery system were synthesized. Spherical poly(HEMA) nanoparticles were produced, as confirmed by FTIR and TEM, within the size range of 97.8 nm to 125.5 nm. Modifications were made to this formulation, through the incorporation of BAC and 3AAPBA, to allow for degradation and mucoadhesion. Poly(HEMA, BAC) and poly(HEMA, BAC, 3AAPBA) nanoparticles were found to have diameters within the range of 227.0 nm to 302.6 nm and 179.5 nm to 219.4 nm, respectively. These nanoparticles were found to be spherical using TEM. Incorporation of 3AAPBA in the poly(HEMA, BAC, 3AAPBA) nanoparticles was confirmed by the FTIR peak corresponding to the out of plane aromatic C-H bending. Degradation of nanoparticles crosslinked with BAC through the addition of a reducing agent, DTT, was observed by TEM and turbidity. TEM showed the poly(HEMA, BAC) and poly(HEMA, BAC, 3AAPBA) nanoparticles reduced to smaller fragments and the turbidity, which was measured indirectly by absorbance, of the nanoparticle suspensions decreased. Poly(HEMA, BAC, 3AAPBA) samples C3 to C6 from Table 3 were found to be mucoadhesive due to the change in the zeta potential after incubation with mucin. Based on the dexamethasone release profiles from poly(HEMA) and poly(HEMA, BAC, 3AAPBA) nanoparticles rate constant of 0.001 and 0.002 and release exponents of 0.607 and 0.586 were obtained, respectively. These rate constants correspond to anomalous transport, a combination of phenomena including diffusion and polymer swelling, being the drug release mechanism. The viability of HCEC after incubation with poly(HEMA),

poly(HEMA, BAC), and poly(HEMA, BAC, 3AAPBA) nanoparticles was 123.6% to 182.5%, 88.5% to 111%, and 69.8% to 85.1%, respectively. Based on these results, there was no significant relationship between HCEC and the concentration of the samples for all samples tested. The HCEC viability was significantly higher for the poly(HEMA) nanoparticles relative to the poly(HEMA, BAC) nanoparticles with a dilution factor of 0 and 2, as well as for the poly(HEMA, BAC, 3AAPBA) samples C2 and C3 relative to sample C6 from Table 3. Overall, the results suggest that these materials have the potential for further development as a drug delivery method for treating diseases of the anterior segment.

Future experimentation should be focused on *in vivo* testing the mucoadhesion of the poly(HEMA, BAC, 3AAPBA) nanoparticle formulations. These studies should be conducted to test the residence time of the poly(HEMA, BAC, 3AAPBA) nanoparticles at the front of the eye. Additionally, the current nanoparticle formulations can be improved by increasing the drug loading efficiency, finding a compatible sterilization technique, and reducing the polydispersity to ensure that the maximum diameter is less than 200 nm.

6. REFERENCES

Acemoglu, M. (2004). Chemistry of polymer biodegradation and implications on parenteral drug delivery. *International journal of pharmaceutics*, *277*(1), 133-139.

Alvarez-Lorenzo, C., Yanez, F., Barreiro-Iglesias, R., & Concheiro, A. (2006). Imprinted soft contact lenses as norfloxacin delivery systems. *Journal of Controlled Release*, *113*(3), 236-244.

Arshady, R. (1992). Suspension, emulsion, and dispersion polymerization: a methodological survey. *Colloid and Polymer Science*, *270*(8), 717-732.

Atchison, D. A., Smith, G., & Smith, G. (2000). Optics of the human eye.

Azari, A. A., & Barney, N. P. (2013). Conjunctivitis: a systematic review of diagnosis and treatment. *Jama*, *310*(16), 1721-1730.

Azevedo, H. S., & Reis, R. L. (2005). Understanding the enzymatic degradation of biodegradable polymers and strategies to control their degradation rate. *Biodegradable systems in tissue engineering and regenerative medicine. Boca Raton, FL: CRC Press*, *177201*.

Bravo-Osuna, I., Vauthier, C., Farabollini, A., Palmieri, G. F., & Ponchel, G. (2007). Mucoadhesion mechanism of chitosan and thiolated chitosan-poly (isobutyl cyanoacrylate) core-shell nanoparticles. *Biomaterials*, *28*(13), 2233-2243.

Bucolo, C., Drago, F., & Salomone, S. (2012). Ocular drug delivery: a clue from nanotechnology. *Frontiers in pharmacology*, *3*, 188.

Cadotte, A. J., & DeMarse, T. B. (2005). Poly-HEMA as a drug delivery device for in vitro neural networks on micro-electrode arrays. *Journal of neural engineering*, *2*(4), 114.

Chirila, T. V., Constable, I. J., Crawford, G. J., Vijayasekaran, S., Thompson, D. E., Chen, Y. C., ... & Griffin, B. J. (1993). Poly (2-hydroxyethyl methacrylate) sponges as implant materials: in vivo and in vitro evaluation of cellular invasion. *Biomaterials*, *14*(1), 26-38.

Chouhan, R., & Bajpai, A. K. (2009). An in vitro release study of 5-fluoro-uracil (5-FU) from swellable poly-(2-hydroxyethyl methacrylate)(PHEMA) nanoparticles. *Journal of Materials Science: Materials in Medicine*, *20*(5), 1103-1114.

Dalton, P. D., & Shoichet, M. S. (2001). Creating porous tubes by centrifugal forces for soft tissue application. Biomaterials, 22(19), 2661-2669.

De Jong, W. H., & Borm, P. J. (2008). Drug delivery and nanoparticles: applications and hazards. *International journal of nanomedicine*, *3*(2), 133.

Deshayes, S., & Kasko, A. M. (2013). Polymeric biomaterials with engineered degradation. *Journal of Polymer Science Part A: Polymer Chemistry*, *51*(17), 3531-3566.

dos Santos, J. F. R., Alvarez-Lorenzo, C., Silva, M., Balsa, L., Couceiro, J., Torres-Labandeira, J. J., & Concheiro, A. (2009). Soft contact lenses functionalized with pendant cyclodextrins for controlled drug delivery. *Biomaterials*, *30*(7), 1348-1355.

Farokhzad, O. C., & Langer, R. (2009). Impact of nanotechnology on drug delivery. *ACS nano*, *3*(1), 16-20.

Ferreira, L., Vidal, M. M., & Gil, M. H. (2000). Evaluation of poly (2-hydroxyethyl methacrylate) gels as drug delivery systems at different pH values. *International journal of pharmaceutics*, *194*(2), 169-180.

Fotakis, G., & Timbrell, J. A. (2006). In vitro cytotoxicity assays: comparison of LDH, neutral red, MTT and protein assay in hepatoma cell lines following exposure to cadmium chloride. *Toxicology letters*, *160*(2), 171-177.

Foster, P. J., Buhrmann, R., Quigley, H. A., & Johnson, G. J. (2002). The definition and classification of glaucoma in prevalence surveys. *British journal of ophthalmology*, *86*(2), 238-242.

Friedlaender, M. H. (1993). Conjunctivitis of allergic origin: clinical presentation and differential diagnosis. *Survey of ophthalmology*, *38*, 105-114.

Garhart, C., & Lakshminarayanan, V. (2012). Anatomy of the Eye. In *Handbook of visual display technology* (pp. 73-83). Springer Berlin Heidelberg.

Gaudana, R., Ananthula, H. K., Parenky, A., & Mitra, A. K. (2010). Ocular drug delivery. *The AAPS journal*, *12*(3), 348-360.

Ghate, D., & Edelhauser, H. F. (2006). Ocular drug delivery.

Garhwal, R., Shady, S. F., Ellis, E. J., Ellis, J. Y., Leahy, C. D., McCarthy, S. P., ... & Gaines, P. (2012). Sustained ocular delivery of ciprofloxacin using nanospheres and conventional contact lens materials. *Investigative ophthalmology & visual science*, *53*(3), 1341-1352.

Gulsen, D., & Chauhan, A. (2004). Ophthalmic drug delivery through contact lenses. *Investigative ophthalmology & visual science*, *45*(7), 2342-2347

Gupta, M. K., Bajpai, J., & Bajpai, A. K. (2014). Preparation and characterizations of superparamagnetic iron oxide-embedded poly (2-hydroxyethyl methacrylate) nanocarriers. *Journal of Applied Polymer Science*, *131*(18).

Holly, F. J., & Refojo, M. F. (1975). Wettability of hydrogels I. Poly (2-hydroxyethyl methacrylate). *Journal of biomedical materials research*, *9*(3), 315-326.

Hombach, J., & Bernkop-Schnürch, A. (2010). Mucoadhesive drug delivery systems. In *Drug Delivery* (pp. 251-266). Springer Berlin Heidelberg.

Hudgins, D. M., & Allamandola, L. J. (1995). Infrared spectroscopy of matrix-isolated polycyclic aromatic hydrocarbon cations. 3. The polyacenes anthracene, tetracene, and pentacene. *The Journal of physical chemistry*, *99*(22), 8978-8986.

Ibrahim, H. K., El-Leithy, I. S., & Makky, A. A. (2010). Mucoadhesive nanoparticles as carrier systems for prolonged ocular delivery of gatifloxacin/prednisolone bitherapy. *Molecular pharmaceutics*, *7*(2), 576-585.

Ivanov, A. E., Solodukhina, N. M., Nilsson, L., Nikitin, M. P., Nikitin, P. I., Zubov, V. P., & Vikhrov, A. A. (2012). Binding of mucin to water-soluble and surface-grafted boronate-containing polymers. Polymer Science Series A, 54(1), 1-10.

Jung, H. J., & Chauhan, A. (2012). Temperature sensitive contact lenses for triggered ophthalmic drug delivery. *Biomaterials*, *33*(7), 2289-2300.

Karakoc, V., Yılmaz, E., Türkmen, D., Öztürk, N., Akgöl, S., & Denizli, A. (2009). Selective separation of human serum albumin with copper (II) chelated poly (hydroxyethyl methacrylate) based nanoparticles. *International journal of biological macromolecules*, *45*(2), 188-193.

Kaur, I. P., Garg, A., Singla, A. K., & Aggarwal, D. (2004). Vesicular systems in ocular drug delivery: an overview. *International journal of pharmaceutics*, *269*(1), 1-14.

Khare, A., Grover, K., Pawar, P., & Singh, I. (2014). Mucoadhesive polymers for enhancing retention in ocular drug delivery: a critical review. *Reviews of Adhesion and Adhesives*, *2*(4), 467-502.

Khutoryanskiy, V. V. (2011). Advances in mucoadhesion and mucoadhesive polymers. *Macromolecular bioscience*, *11*(6), 748-764.

Kiel, J. W. (2010). Local control of ocular blood flow.

Lee, S. S., Hughes, P., Ross, A. D., & Robinson, M. R. (2010). Biodegradable implants for sustained drug release in the eye. *Pharmaceutical research*, *27*(10), 2043-2053.

Lehr, C. M., Bouwstra, J. A., Schacht, E. H., & Junginger, H. E. (1992). In vitro evaluation of mucoadhesive properties of chitosan and some other natural polymers. *International journal of Pharmaceutics*, *78*(1), 43-48.

Lemp, M. A., & Foulks, G. N. (2007). The definition and classification of dry eye disease. *The Ocular Surface*, *5*(2), 75-92.

Leske, M. C. (1983). The epidemiology of open-angle glaucoma: a review. *American journal of epidemiology*, *118*(2), 166-191.

Lou, X., Munro, S., & Wang, S. (2004). Drug release characteristics of phase separation pHEMA sponge materials. *Biomaterials*, *25*(20), 5071-5080.

Ludwig, A. (2005). The use of mucoadhesive polymers in ocular drug delivery. *Advanced drug delivery reviews*, *57*(11), 1595-1639.

McCannel, C. A., Holland, G. N., Helm, C. J., Cornell, P. J., Winston, J. V., Rimmer, T. G., & UCLA Community-Based Uveitis Study Group. (1996). Causes of uveitis in the general practice of ophthalmology. *American journal of ophthalmology*, *121*(1), 35-46.

Meng, F., Hennink, W. E., & Zhong, Z. (2009). Reduction-sensitive polymers and bioconjugates for biomedical applications. *Biomaterials*, *30*(12), 2180-2198.

Montheard, J. P., Chatzopoulos, M., & Chappard, D. (1992). 2-hydroxyethyl methacrylate (HEMA): chemical properties and applications in biomedical fields. *Journal of Macromolecular Science, Part C: Polymer Reviews*, *32*(1), 1-34.

Nagpal, K., Singh, S. K., & Mishra, D. N. (2010). Chitosan nanoparticles: a promising system in novel drug delivery. *Chemical and Pharmaceutical Bulletin*, *58*(11), 1423-1430.

Nicolson, P. C., & Vogt, J. (2001). Soft contact lens polymers: an evolution. *Biomaterials*, *22*(24), 3273-3283.

Öztürk, N., Bereli, N., Akgöl, S., & Denizli, A. (2008). High capacity binding of antibodies by poly (hydroxyethyl methacrylate) nanoparticles. *Colloids and Surfaces B: Biointerfaces*, *67*(1), 14-19.

Peppas, N. A., Moynihan, H. J., & Lucht, L. M. (1985). The structure of highly crosslinked poly (2-hydroxyethyl methacrylate) hydrogels. *Journal of biomedical materials research*, *19*(4), 397-411.

Perova, T. S., Vij, J. K., & Xu, H. (1997). Fourier transform infrared study of poly (2-hydroxyethyl methacrylate) PHEMA. Colloid and Polymer Science, 275(4), 323-332.

Phan, C. M., Subbaraman, L., Liu, S., Gu, F., & Jones, L. (2014). In vitro uptake and release of natamycin Dex-b-PLA nanoparticles from model contact lens materials. *Journal of Biomaterials Science, Polymer Edition*, *25*(1), 18-31.

Purves, D., Augustine, G. J., Fitzpatrick, D., Katz, L. C., LaMantia, A. S., McNamara, J. O., & Williams, S. M. (2001). Anatomy of the Eye.

Schäfer-Korting, M. (Ed.). (2010). *Drug delivery* (Vol. 197). Springer Science & Business Media.

Siepmann, J., & Siepmann, F. (2008). Mathematical modeling of drug delivery. *International journal of pharmaceutics*, *364*(2), 328-343.

Singhvi, G., & Singh, M. (2011). Review: in-vitro drug release characterization models. *Int J Pharm Stud Res*, *2*(1), 77-84.

Smart, J. D. (2005). The basics and underlying mechanisms of mucoadhesion. *Advanced drug delivery reviews*, *57*(11), 1556-1568.

Smerdon, D. (2000). Anatomy of the eye and orbit. *Current Anaesthesia & Critical Care*, *11*(6), 286-292.

Soppimath, K. S., Aminabhavi, T. M., Kulkarni, A. R., & Rudzinski, W. E. (2001). Biodegradable polymeric nanoparticles as drug delivery devices. *Journal of controlled release*, *70*(1), 1-20.

Türkcan, C., Akgöl, S., & Denizli, A. (2013). Silanized polymeric nanoparticles for DNA isolation. *Materials Science and Engineering: C*, *33*(8), 4498-4503.

Urtti, A. (2006). Challenges and obstacles of ocular pharmacokinetics and drug delivery. *Advanced drug delivery reviews*, *58*(11), 1131-1135.

Uygun, M., Uygun, D. A., Altunbaş, C., Akgöl, S., & Denizli, A. (2014). Dye Attached Nanoparticles for Lysozyme Adsorption. *Separation Science and Technology*, *49*(8), 1270-1278.

Wadhwa, S., Paliwal, R., Paliwal, S. R., & Vyas, S. P. (2010). Hyaluronic acid modified chitosan nanoparticles for effective management of glaucoma: development, characterization, and evaluation. *Journal of drug targeting*, *18*(4), 292-302.

Weisstein, E. W. (2002). Least squares fitting.

Withers, C. A., Cook, M. T., Methven, L., Gosney, M. A., & Khutoryanskiy, V. V. (2013). Investigation of milk proteins binding to the oral mucosa. Food & function, 4(11), 1668-1674.

Xu, J., Li, X., & Sun, F. (2010). Cyclodextrin-containing hydrogels for contact lenses as a platform for drug incorporation and release. *Acta Biomaterialia*, *6*(2), 486-493.

Young, C. D., Wu, J. R., & Tsou, T. L. (1998). High-strength, ultra-thin and fiber-reinforced pHEMA artificial skin. *Biomaterials*, *19*(19), 1745-1752.

Zaikov, G. E. (1985). Quantitative aspects of polymer degradation in the living body. Journal of Macromolecular Science-Reviews in Macromolecular Chemistry and Physics, 25(4), 551-597.

Zaikov, G. E., & Horák, D. (2007). *Polymers and Composites: Synthesis, Properties and Applications*. Nova Publishers.

Zhang, X., Wang, Y., Zheng, C., & Li, C. (2012). Phenylboronic acid-functionalized glycopolymeric nanoparticles for biomacromolecules delivery across nasal respiratory. *European Journal of Pharmaceutics and Biopharmaceutics*, *82*(1), 76-84.

APPENDIX A

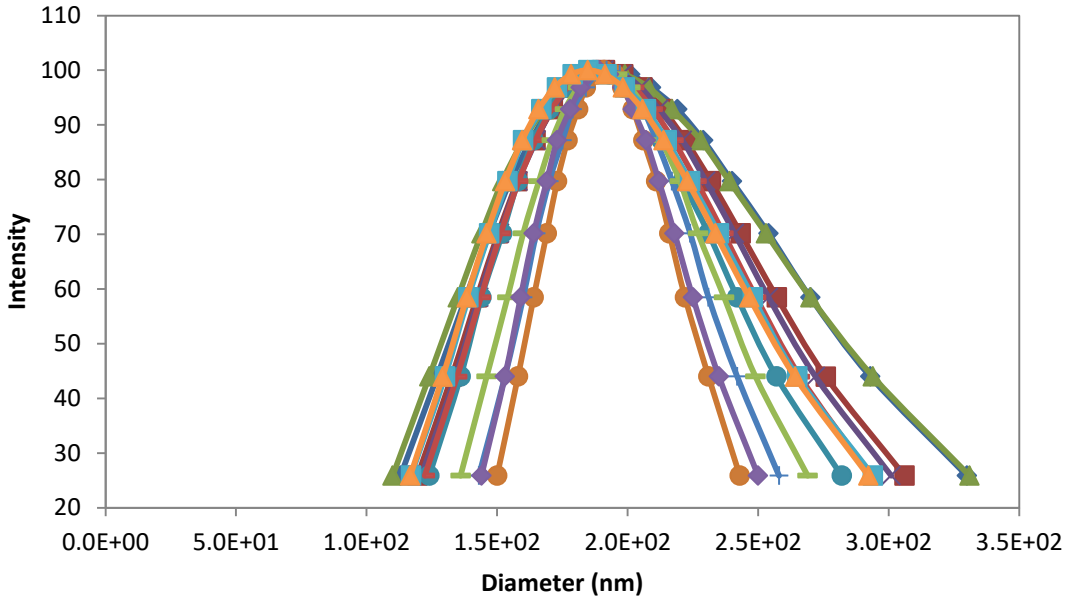

Figure A1. Log normal particle size distribution of poly(HEMA, BAC, 3AAPBA) sample C2 from Table 3. The lines correspond to measurements 1 (◆), 2 (■), 3 (▲), 4 (×), 5 (●), 6 (●), 7 (+), 8 (—), 9 (—), 10 (◆), 11 (■), 12 (▲).

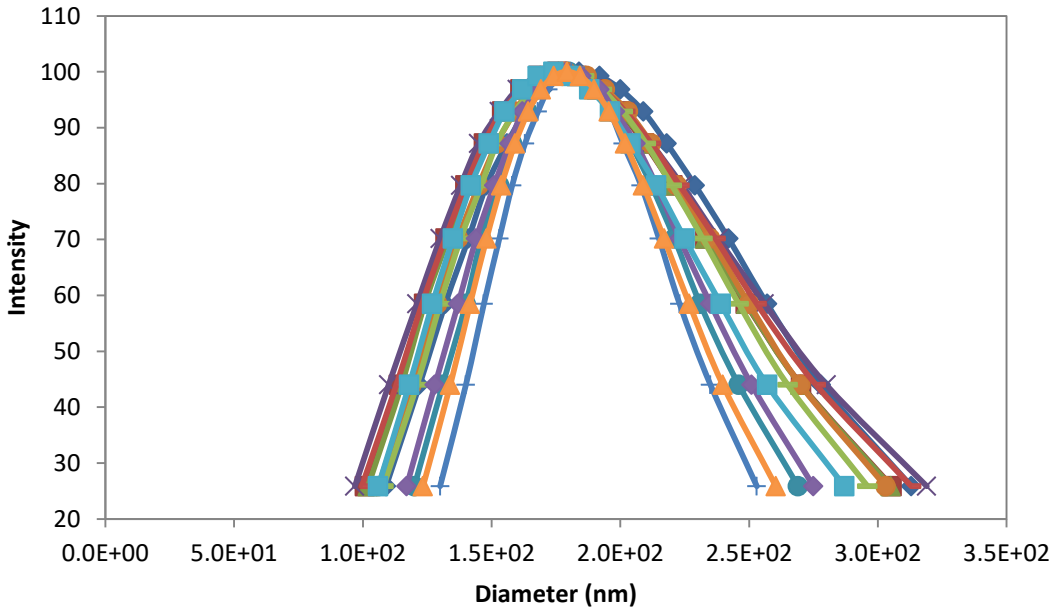

Figure A2. Log normal particle size distribution of poly(HEMA, BAC, 3AAPBA) sample C4 from Table 3. The lines correspond to measurements 1 (◆), 2 (■), 3 (▲), 4 (×), 5 (●), 6 (●), 7 (+), 8 (—), 9 (—), 10 (◆), 11 (■), 12 (▲).

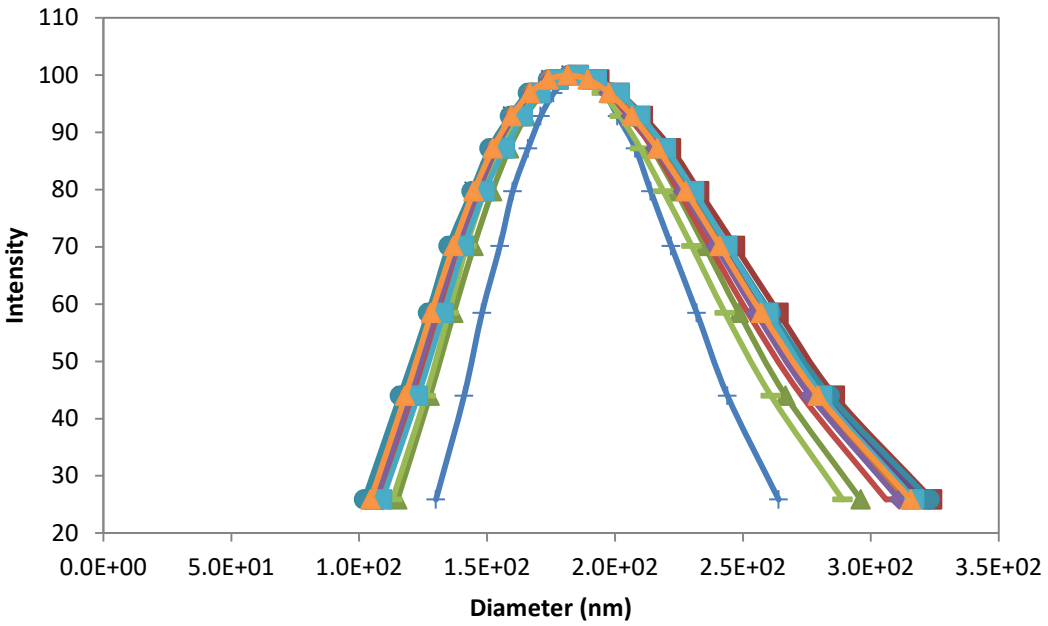

Figure A3. Log normal particle size distribution of poly(HEMA, BAC, 3AAPBA) sample C5 from Table 3. The lines correspond to measurements 1 (◆), 2 (■), 3 (▲), 4 (×), 5 (●), 6 (●), 7 (+), 8 (—), 9 (—), 10 (◆), 11 (■), 12 (▲).

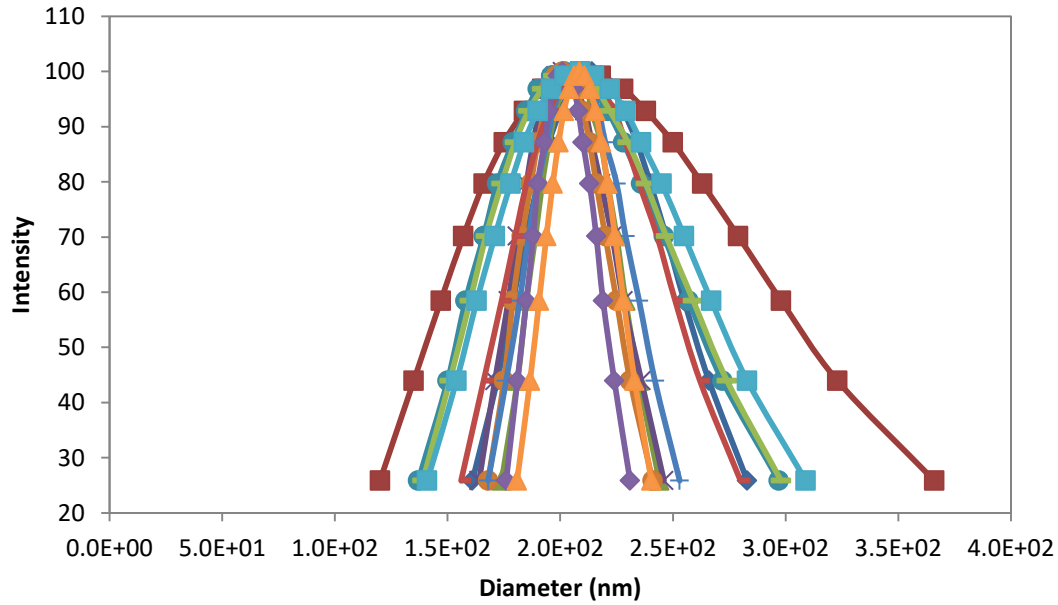

Figure A4. Log normal particle size distribution of poly(HEMA, BAC, 3AAPBA) sample C6 from Table 3. The lines correspond to measurements 1 (◆), 2 (■), 3 (▲), 4 (×), 5 (●), 6 (●), 7 (+), 8 (—), 9 (—), 10 (◆), 11 (■), 12 (▲).